Plasmacytoid Dendritic Cells and Infected Cells Form an Interferogenic Synapse Required for Antiviral Responses

Sonia Assil, Séverin Coléon, Congcong Dong, Elodie Décembre, Lee Sherry, Omran Allatif, Brian Webster, Marlène Dreux

Plasmacytoid Dendritic Cells and Infected Cells form an Interferogenic Synapse Required for Antiviral Responses

Sonia Assil[1*], Séverin Coléon[1*], Congcong Dong[1], Elodie Décembre[1], Lee Sherry[1], Omran Allatif[1], Brian Webster[1] and Marlène Dreux[1, 2]

1 CIRI, Inserm, U1111, Université Claude Bernard Lyon 1, CNRS, UMR5308, École Normale Supérieure de Lyon, Univ Lyon, F-69007, LYON, France

2 Corresponding author/lead contact; email: marlene.dreux@ens-lyon.fr, Tel.: + +33 426 23 38 34.

* These authors contributed equally

Running title: pDC activation by interferogenic synapse with infected cells

7 Figures; 7 Supplementary Figures

Text: 58 017 characters including Introduction, Results, Discussion; Figure legends; References.

Summary

Type I interferon (IFN-I) is critical for antiviral defense, and plasmacytoid dendritic cells (pDCs) are a predominant source of IFN-I during virus infection. pDC-mediated antiviral responses are stimulated upon physical contact with infected cells, during which immunostimulatory viral RNA is transferred to pDCs, leading to IFN production via the nucleic acid sensor TLR7. Using dengue, hepatitis C, and Zika viruses, we demonstrate that the contact site of pDCs with infected cells is a specialized platform, we term the interferogenic synapse, which enables viral RNA transfer and antiviral responses. This synapse is formed *via* $\alpha_L\beta_2$ integrin/ICAM-1 adhesion complexes and the recruitment of the actin network and endocytic machinery. TLR7 signaling in pDCs promotes interferogenic synapse establishment and provides feed-forward regulation sustaining pDC contacts with infected cells. This interferogenic synapse may allow pDCs to scan infected cells and locally secrete IFN-I, thereby confining a potentially deleterious response.

Introduction

Type I interferon (*i.e.,* IFNα/β, referred to as IFN-I) response is pivotal for protection against viral infections. It is initiated by the recognition of pathogen-associated molecular patterns (PAMPs) including viral nucleic acids by cellular pathogen recognition receptors (PRRs) such as toll-like receptors (TLRs). This leads to the secretion of IFN-I, type III IFNs, inflammatory cytokines and to the expression of an array of IFN-stimulated genes (ISGs) (Hoffmann et al., 2015). This first line of host response suppresses viral spread and jump-starts the adaptive immune response.

All cells possess signaling pathways designed to trigger antiviral responses against invading viruses. Nonetheless, virtually all viruses have evolved mechanisms to inhibit these host-sensing pathways within cells that they infect (Garcia-Sastre, 2017). For example, hepatitis C (HCV), dengue (DENV) and Zika (ZIKV) viruses encode viral proteases, which inactivate the adaptors of host antiviral sensing (Garcia-Sastre, 2017). Despite viral countermeasures, cytokines and ISGs are detected in infected humans and play pivotal roles in infection clearance and pathogenicity, suggesting the existence of alternative pathogen-sensing mechanisms (Martina et al., 2009; Snell et al., 2017; Webster et al., 2016). Along this line, we and others uncovered that plasmacytoid dendritic cells (pDCs) produce robust levels of IFN-I in response to physical contact with infected cells (Webster et al., 2016). This response is unopposed by viral products as pDCs are not productively infected.

pDCs function as sentinels of viral infections and are a major early source of IFN-I *in vivo* during viral infections (Swiecki and Colonna, 2015). This response is predominantly triggered *via* recognition of viral RNA and DNA species by endolysosome-localized TLR7 and TLR9,

respectively. pDC response is pivotal for control of viral infection as recently demonstrated *e.g.,* for DENV (Swiecki and Colonna, 2015; Webster et al., 2018). IFN-I production by pDCs also contributes to several autoimmune or inflammatory diseases, and pDCs are pivotal in cancers (Swiecki and Colonna, 2015). Despite this large spectrum of regulatory functions of pDCs, the molecular bases controlling their activation are still largely enigmatic.

We previously demonstrated that immunostimulatory viral RNA can be transferred by non-canonical/non-infectious carriers from infected cells to pDCs, leading to IFN production *via* the TLR7 sensor. These PAMP-carriers include exosomes and immature viral particles in the context of HCV and DENV, respectively (Decembre et al., 2014; Dreux et al., 2012). The activation of pDCs by exosomal transfer of viral RNA has been also shown for the sensing of genetically distant viruses (Feng et al., 2014; Wieland et al., 2014).

Importantly, while various types of carrier can transfer PAMPs, these pDC activations require physical contact with infected cells (Webster et al., 2016). For example, HCV infected cells secrete exosomes into the culture supernatant at concentrations that are below an excitatory threshold that could be reached in the intercellular space during cell contacts (Dreux et al., 2012). In the context of DENV, viral components (*i.e.* envelope proteins) accumulate at the cell contact between infected cells and pDCs (Decembre et al., 2014). Albeit not universal, the cell contact is increasingly recognized as a requirement for pDC-mediated antiviral state triggered by many genetically distant RNA viruses (*e.g., Flaviviridae, Picornaviridae, Arenaviridae, Retroviridae, Togaviridae*) and in different species (Bruni et al., 2015; Decembre et al., 2014; Dreux et al., 2012; Feng et al., 2014; Garcia-Nicolas et al., 2016; Lepelley et al., 2011; Takahashi et al., 2010; Webster et al., 2016; Webster et al., 2018;

Wieland et al., 2014), nonetheless how the cell contact mediates pDC response is still largely unknown.

Here, we explored the molecular mechanisms underlying the establishment of contacts between pDCs and infected cells, its modulation and impact on the activation of an antiviral state using DENV, HCV and ZIKV as viral models. Our results uncovered that pDCs established cell adhesion with infected cells *via* $\alpha_L\beta_2$ integrin complex and ICAM-1. We showed that regulators of actin network polarized together with components of the endocytosis machinery at contact sites. These actin-mediated reorganizations define a remodeled territory acting as a platform for the transfer of PAMP-carriers to the endolysosomal TLR7, leading to pDC-mediated antiviral response. We further demonstrated that the molecular rearrangements at contact sites were potentiated by the TLR7-mediated response, which thus acts as a positive feed-forward regulation of pDC activation. The formation of interferogenic synapse is thus a pDC attribute critical for their robust IFN response.

Results

The $\alpha_L\beta_2$ integrin/ICAM-1 adhesion molecules are involved in pDC activation by contacts with DENV infected cells

The pDC response to many viruses requires contact, so we sought to define the molecular basis for establishment of physical contacts between pDCs and infected cells. We tested whether cell adhesion complexes can establish pDC/infected cell contact leading to pDC activation. We analyzed the surface expression of selected representatives of cell adhesion/homing complexes, known to be key for pDC functions, *e.g.,* migration and antigen

presentation (Sozzani et al., 2010; Swiecki and Colonna, 2015). L-selectin (CD62L), α_L integrin (ITGAL, CD11a) and intercellular adhesion molecule (ICAM)-1 (CD54) were all expressed at the pDC surface (**Figure S1A**). ICAM-1 was also present at the surface of the donor cells (*i.e.,* infected and uninfected cells), while E-cadherin was present only on donor cell surface (**Figure S1A**). Next we tested the role of cell adhesion molecules in pDC IFNα production induced by contact with DENV infected cells in antibody-mediated blocking assays. The blockade of L-selectin and E-cadherin had no significant impact on pDC IFNα production induced by DENV infected cells (**Figure 1A and S1B)**. In sharp contrast, inhibition of both α_L integrin and its ligand ICAM-1 (Rothlein et al., 1986) prevented the pDC IFNα response in a dose-dependent manner, along with production of IFNβ and type III IFNs (IL-29/28A/28B) (**Figure 1A-B and S1B-C**). Viral infectivity and RNA levels were maintained upon similar treatment of infected cells in absence of pDCs, thus ruling out non-specific effects on DENV replication (**Figure 1A, S1B-C**). The regulation of the establishment of pDC-infected cell contacts by the α_L integrin and its ligand ICAM-1 was determined by imaging flow cytometry technology (**Figure S1D**). We showed that blocking of both α_L integrin and ICAM-1 significantly prevented contacts of pDCs with DENV infected cells (**Figure 1C**).

Next, to define how the pDC response to contact with DENV infected cells inhibits viral propagation, we set-up an assay consisting of pDCs cocultured with GFP^-/DENV infected cells and GFP^+/uninfected cells. The results demonstrated that pDC response readily prevented viral spread from GFP^-/DENV infected cells to the cocultured GFP^+/uninfected cells, and consistently diminished the replication in GFP^- cells, *i.e.,* infected prior to the coculture (**Figure 1D-E**). The inhibition of pDC/infected contact *via* blockage of the α_L integrin restored the viral propagation to levels comparable to those in the absence of pDC

(**Figure 1D-E**). Consistently, the analysis of infectious virus production by DENV infected cells demonstrated similar inhibition by cocultured pDCs (compared to the absence of pDCs) and the restoration of the viral production upon inhibition of α_L integrin (**Figure 1F**). This indicates that the establishment of cell-contact *via* adhesion molecules is required for pDC-mediated antiviral response.

Further, we assessed the impact of silencing ICAM-1 expression in infected cells. pDC IFNα production was strongly reduced when ICAM-1 expression was silenced in DENV infected cells (**Figure 1G-H)**. In absence of pDC, reduced ICAM-1 expression has no impact on virus replication, yet slightly diminished the release of DENV (**Figure 1H**). Although we cannot formally exclude that decreased viral production could contribute to lower pDC activation, pDC IFNα production was disproportionally reduced when ICAM-1 expression was silenced in cocultured infected cells (**Figure 1H)**. Of note, this is in accordance with the results obtained with ICAM-1 blocking antibody suggesting a regulation by ICAM-1 independent of viral production (**Figure 1A and S1B-C**). Together, our results identified α_L integrin/ICAM-1 as a key cell adhesion complex for the sensing of DENV infected cells by pDC leading to a potent antiviral response.

Cell polarity of the adhesion molecules at the pDC/DENV infected cells contact

Next we demonstrated that α_L integrin specifically accumulated at the contact site of pDC/DENV infected cell (*i.e.,* over 90% of the analyzed contacts), as opposed to marginal accumulation at contact of CD123, a surface molecule not involved in cell adhesion (**Figure 2A-C and S2A-B**). The α_L integrin forms complex with β_2 integrin, which is known to undergo conformational rearrangement to an open form compatible with high-affinity interaction with its ligands, including ICAM-1 (Shimaoka et al., 2003). The open/high-

affinity conformation of $\alpha_L\beta_2$ integrin complex polarized at the contact site of pDC/infected cell on the pDC side (**Figure 2D-F and S2C-D**). Of note, cell polarity of α_L integrin and the high-affinity conformation of $\alpha_L\beta_2$ integrin complex was absent when pDCs were not in contact with infected cells, shown by the quantification of α_L integrin accumulation *versus* diffuse localization around the pDCs (**Figure 2G-I and S2E-F**), and thus validating the specificity of the polarization upon cell contact. Further, in agreement with the engagement of the $\alpha_L\beta_2$ integrin complex with its ligand, ICAM-1, the latter was detected at contact on the surface of infected cells apposed to polarized α_L integrin on pDC side (**Figure 2J-L**). Our results demonstrate that the open/high affinity conformation $\alpha_L\beta_2$ integrin complex accumulates at contact, facing its partner ICAM-1.

The $\alpha_L\beta_2$ integrin/ICAM-1 adhesion molecules are required for pDC activation by distinct viruses

The activation of pDCs by HCV infected cells also requires physical contact, yet this involves a distinct PAMP-carrier *i.e.,* exosome (*versus* immature viral particles for DENV) (Decembre et al., 2014; Dreux et al., 2012). We thus tested whether $\alpha_L\beta_2$ integrin/ICAM-1 adhesion complexes were also required for pDC activation by HCV infected cells. Similar to DENV, ICAM-1 is present at the surface of HCV infected cells (**Figure S3D**) and blocking of both α_L integrin and ICAM-1 diminished the pDC IFNα response to HCV infected cells, in dose-response experiments, without any non-specific effect on HCV viral production - in absence of pDC (**Figure 3A and S3A**). Consistently, blocking both α_L integrin and ICAM-1 significantly prevented contacts of pDCs with HCV infected cells (**Figure 3B**). Although the presence of ICAM-1 on PAMP-carriers could additionally contribute to their tethering to the surface of the pDCs, altogether these results demonstrated that the $\alpha_L\beta_2$ integrin/ICAM-1 interaction regulates the formation of pDC-infected cell conjugate and are required for pDC

activation, independently of the nature of PAMP-carrier. In sharp contrast, anti-α_L integrin and anti-ICAM-1 did not prevent pDC IFNα production triggered by cell-free virus *i.e.,* influenza virus (**Figure 3C**), suggesting that $\alpha_L\beta_2$ integrin/ICAM-1 interaction regulates cell contact mediated-pDC activation.

Next we extended our demonstration to ZIKV, which also represents an important health concern (Miner and Diamond, 2017). Using epidemic ZIKV strains (*i.e.,* isolated from patients in Brazil and French Polynesia; H/PF), we demonstrated that robust pDC IFNα productions were induced when pDCs were in physical contact with ZIKV infected cells (**Figure 3D**; coculture set-up). On the contrary, no IFNα response was detected when pDCs were exposed to ZIKV infectious supernatants (SN) or upon physical separation of pDCs from ZIKV infected cells by a semi-permeable membrane in transwell (TW) experiments (**Figure 3D**). In accordance with TLR7 localized in endolysosome, and like DENV/HCV, pDC activation by ZIKV infected cells involved endocytosis (**Figure S3B**). Importantly, we showed that, similar to what is observed for DENV/HCV, pDC response to ZIKV infected cells is mediated by α_L integrin/ICAM-1 adhesion molecules as shown by the reduced production of IFNα, IFNβ and type III IFNs by antibody blocking (**Figure 3F-G, S3C and S3E**).

Next, we demonstrated that, similar to the observation with DENV, pDC response to contact with ZIKV infected cells prevented ZIKV transmission to uninfected cells (GFP^+), replication in the cells infected prior to coculture (GFP^-) and viral production (**Figure 3H-I and S3F**). Of note, the inhibition of α_L integrin in infected cell/pDC cocultures greatly restored viral propagation to levels similar to those in the absence of pDCs (**Figure 3H-I and S3F**), indicated that the establishment of cell-contact is required for pDC-mediated antiviral

response against ZIKV. Together, our results demonstrate that the establishment of pDC/infected cell interactions *via* cell adhesion complex is a prerequisite for the antiviral function of pDC in response to cells infected by distinct viruses.

Polarization at contact site of actin network and regulators contribute to pDC response

The engagement of integrins with their ligand can induce the local recruitment of the actin network, notably *via* Arp2/3 complex, which mediate actin nucleation by branching of the actin filaments within network (DeMali et al., 2002; DeMali et al., 2014; Rotty et al., 2013; Vicente-Manzanares et al., 2009). This is in line with our preceding observations for the presence of actin at pDC/DENV infected cell contact (Decembre et al., 2014). Here, we showed that actin network accumulated at cell contacts, using both HCV infected cells and the subgenomic replicon (SGR) model for HCV replication (**Figure S4A-D**). HCV SGR cells do not produce virus but trigger pDC IFN response, as previously reported (Dreux et al., 2012; Takahashi et al., 2010) and thus demonstrating that cell polarity at contact is independent of viral production (**Figure S4A-B)**. Non-specific polarized immunodetection was ruled out by the simultaneous analysis of another intracellular component, the protein disulfide-isomerase (PDI), an ER marker and by the expected decrease of actin clustering upon treatment with inhibitor of actin polymerization *i.e.,* Latrunculin B (**Figure S4B, D**).

We thus sought to define the subcellular localization of key regulators of actin network scaffolding at the plasma membrane. We first selected the phosphatidylinositol 4,5 biphosphate ($PI(4,5)P_2$) because it is a plasma membrane-localized modified lipid known to recruit actin-adaptor proteins and to regulate the clustering of integrins as well as clathrin-mediated endocytosis (Jost et al., 1998; Martel et al., 2001; Posor et al., 2015; Vicente-Manzanares et al., 2009). The type I phosphatidylinositol-4-phosphate-5-kinase α (referred to

as PIP5KIα) generates PI(4,5)P_2 from its PI4P precursor (Doughman et al., 2003). We showed that PI(4,5)P_2 and PIP5KIα co-clustered at the contact sites of pDCs with cells infected either by DENV or HCV, or with HCV replicating (rep) cells (**Figure 4A-L**). The 3D-reconstruction of consecutive Z-stacks further revealed that the co-clusters were present on the side of pDCs (**Figure 4C, G, K**). The quantification of PI(4,5)P_2/PIP5KIα co-clustering revealed that intact actin network was required for the polarization at contact, as demonstrated by the decrease in phenotype when using inhibitors of Arp2/3 complex and actin polymerization (**Figure 4D, H, L**). Of note, the frequency of PI(4,5)P_2/PIP5KIα co-clustering at pDC/infected cell contacts was lower compared to the polarization of the α_L integrin (**Figure 2C and 2I**), likely reflecting the transient nature and/or differential kinetics of these recruitments at contact as compared to the adhesion complexes.

Next, we tested the functional role of actin network regulators, including Arp2/3 complex, and the Rho GTPase CDC42, which also regulates actin polymerization, and along with PI(4,5)P_2, is known to induce actin nucleation *via* Arp2/3 (Higgs and Pollard, 2000; Rohatgi et al., 1999; Rozelle et al., 2000). The pharmacological inhibition of either Arp2/3 complex, CDC42 or actin polymerization prevented pDC IFNα production induced by DENV or HCV infected cells, without non-specific effect on the viral replication of DENV and HCV in absence of pDC (**Figure 4M-O, S4E-G and S4I-L**). Of note, similar pharmacological inhibition of Arp2/3 did not prevent pDC IFNα production triggered by cell-free influenza virus (**Figure 4P**), implying that Arp2/3-mediated actin nucleation is pivotal for pDC response induced by contact with infected cells. This assumption was validated by the reduced frequency of pDC/infected cell contacts upon inhibition of Arp2/3 and actin polymerization (**Figure 4Q-R and S4H**). Our results underscore that integrin-mediated adhesion and rearrangement at contact of actin network *via* notably Arp2/3, are pivotal for the

establishment and/or reinforcement of the cell contacts with infected cells and subsequent pDC activation, presumably by a concerted structuring of the contact site.

Components of the endocytosis machinery polarize at contacts

The immunostimulatory viral RNAs are transferred by vesicles (*i.e.,* exosome or immature virion) from infected cells to pDCs and induce IFN-I response *via* clathrin-mediated endocytosis by pDCs and recognition through endolysosome-localized TLR7 (**Figure S3B**) (Decembre et al., 2014; Dreux et al., 2012; Takahashi et al., 2010; Webster et al., 2016). Of note, $PI(4,5)P_2$, which clustered at contact (**Figure 4A-L**) is known to mark the plasma membrane and, together with cargo proteins, is pivotal for the initiation of clathrin-coated pit formation and consistently, PIP5KIα *via* $PI(4,5)P_2$ synthesis control the rate and growth of clathrin-coated pits (Jost et al., 1998; Posor et al., 2015). We thus tested whether the components of the endocytosis machinery could polarize at contact and thereby facilitate the internalization of PAMP-carriers by pDCs. We observed co-clusters of $PI(4,5)P_2$ and Early Endosome Antigen 1 (EEA1) at the contact sites of pDCs with DENV infected cells, and similarly with HCV replicating cells (**Figure 5A-F, 5J-K and S5A-B**). The 3D-reconstruction of consecutive Z-stack imaging suggested that the $PI(4,5)P_2$/EEA1 co-clustering was present on the pDC side of the contact (**Figure 5C and 5F**). Similarly, clathrin co-clustered with actin on the pDC side, as revealed by the 3D-reconstruction of contact sites (**Figure 5G-I, 5L and S5C-F)**. The cell polarity of both these markers at contact required an intact actin network, as demonstrated by using inhibitors of Ap2/3 complex and actin polymerization (**Figure 5J-L**). Together our results suggest that components of the endocytosis machinery polarize at the contact between pDCs and infected cells, thus representing a functional remodeling to favor a localized endocytosis of PAMP-carriers leading to pDC activation *via* the endolysosomal TLR7.

TLR7-induced pDCs establish sustained contact with virally infected cells

The rearrangement of the contact site into a specialized territory on the side of pDCs suggests the existence of a dynamic process within pDCs when in contact and sensing infected cells. We hypothesized that the sensing by pDCs of PAMP-carriers released by infected cells, and thereby the activated state of the pDCs could control the contact establishment and/or the polarization of pDC cellular machineries. The frequency of pDCs conjugated with infected cells was significantly higher as compared to uninfected cells (**Figure 6A**). Similar results were obtained for DENV and HCV infected cells, thus showing that the potentiation of contacts by sensing of virally infected cells is not virus-restricted.

To further demonstrate that pDC contact with infected cells are more stable compared to uninfected cells, we developed a live-imaging approach (using spinning-disk confocal microscopy) to quantify the duration of pDC contact with infected cells as compared to uninfected cells (**Figure S6A**). Distinct categories of contact duration were observed, including short-lived contacts (<100 min), intermediate duration contacts of low frequencies and sustained contact (>350 min) (**Figure 6B-I**). Importantly, the frequency of long-lasting contacts was higher when pDCs were cocultured with DENV infected cells as compared to contact with uninfected cells (**Figure 6B and 6F**). In accordance, as highlighted in tracking motion analysis pDC motility, and consistently the number of contact per pDCs, were reduced when cocultured with infected as compared to uninfected cells (**Figure S6B-C** and **S6K**). Similar results were obtained in the context of pDC cocultured with HCV replicating cells (**Figure 6C and 6G**), suggesting this regulation is not virus-restricted and independent of the type of PAMP-carriers. Live-imaging experiments with blocking anti-α_L integrin revealed that the long-lasting contacts with infected cells involved α_L integrin (**Figure 6D, 6H and S6E**).

Furthermore, the blocking anti-α_L integrin decreased the frequency of conjugates even when added later in course of pDC/infected cell coculture and leading to reduced IFNα production by pDCs (**Figure S6G-I**).

Our results demonstrated that pDCs established sustained contact with infected cells, thus implying that a molecular regulation of the contact by either sensing of the infected status of cells and/or the activating state of pDCs promotes their retention at the contact of infected cells. We thus tested the regulation of the pDC/infected cell contact by TLR7-induced signaling. To address this question, we used a specific TLR7 inhibitor (*i.e.,* IRS661), which diminished the pDC IFNα production induced by DENV infected cells, as previously reported (Decembre et al., 2014). We found that the inhibition of TLR7 signaling diminished the frequency of the long-lived contacts of pDCs with infected cells (**Figure 6B, 6F and S6D**). Inhibition of TLR7 signaling thus reverted the duration of pDC contacts to those observed with uninfected cells. Accordingly, TLR7 agonist increased the frequency of long-lasting contact of pDCs with non-infected cells, without a marked impact on pDC velocity (**Figure 6E, 6I, S6F, S6J and S6L-M**). Altogether our results demonstrate that TLR7-signaling induced by recognition of infected cells exerts a feed-forward regulation leading to sustained contact of pDCs with infected cells.

Recognition of viral infection favors polarization of cellular components at contacts via TLR7-induced signaling

Next, we tested whether the sustained contact observed with infected cells was associated with increased polarization of the identified cell adhesion molecules at the contact sites. The total surface expression of ICAM-1 did not markedly change when comparing uninfected

versus cells infected by the different viral models (**Figure S1A and S3D**), neither did the level of α_L integrin on pDC cell surface when cocultured with either infected or uninfected cells (**Figure S7A-B)**. Importantly, the co-accumulation at contact of $\alpha_L$integrin/ICAM-1 significantly augmented when pDCs were in contact with DENV or HCV infected cells as compared to uninfected cells (**Figure 7A-B**). In accordance with the known interplay between $\alpha_L$integrin/ICAM-1 and actin network/regulators (DeMali et al., 2014), we showed that the polarization of actin network regulators including PI(4,5)P_2/PIP5KIα increased upon contact with DENV infected cells and similarly for HCV infected and HCV replicating cells (**Figure 7C, 7F, 7I**).

We demonstrated that the inhibition of TLR7-induced signaling prevented the establishment of long-lived contact of pDCs with infected cells (**Figure 6B and 6F**). By analogy to inside-out signaling defined in the context of other cell contact including neurological and immunological synapses (Hogg et al., 2011; Park and Goda, 2016), we hypothesized that TLR7-induced signaling might promote the cell polarity. We showed that the inhibition of TLR7 significantly reduced coclustering of PI(4,5)P_2/PIP5KIα at contact, along with endocytosis components, including the coclustering of PI(4,5)P_2/EEA1 and clathrin/actin (**Figure 7C-D, 7F-G, 7I-L**). The coclusters of α_L integrin and the high-affinity conformation of $\alpha_L\beta_2$ integrin complex together with the endocytosis components (*i.e.,* clathrin and EEA1, respectively) at the contact site of pDCs were also subjected to regulation by TLR7-mediated pDC activation (**Figure 7E, 7H and S7C-D**). This further implies a connection between components of the cell adhesion, actin network and the endocytosis machinery modulated by TLR7 signaling. Similar results were obtained using DENV, HCV and ZIKV infected cells (**Figure 7 and S7**), highlighting that the control by TLR7-mediated signaling of pDC polarity is neither restricted to specific virus nor PAMP-carrier. Our results demonstrate that the

sensing of infected cells *via* TLR7 sensor induces cell polarity of regulators of adhesion, actin network and endocytosis machinery at contact on the pDC side, thus acting as a positive feedback regulation for the efficient transfer of PAMP-carriers and pDC response.

Discussion

pDCs are important mediators of IFN-I response. We demonstrate that pDC activation is mediated by the establishment of sustained contact with infected cells *via* cell adhesion molecules, $\alpha_L\beta_2$ integrin complex and ICAM-1. This is associated with the polarization of the actin network and its regulators as well as components of the endocytosis machinery, at the contact site within pDCs, requiring and facilitating sensing of viral RNA by endolysosome-localized-TLR7. Furthermore, we provide compelling evidence that TLR7-induced signaling in pDCs regulates the rearrangement of a polarized platform at contact site and prolongs cell contacts, thus acting as a feed-forward regulation for the transfer of PAMP-carrier to the pDCs. Cell polarity is thus a previously unappreciated primary attribute of pDCs necessary to sense virally infected cells and respond by a robust antiviral response, which prevents viral spread. We propose to call this functional structuring the interferogenic synapse, by analogy to previously described synapses, while functionally driving a distinct cellular response.

PAMP transfer *via* physical contact and cell polarity: the interferogenic synapse

Different types of synapses have been defined including neurological, immunological and virological synapses, which differ in composition and signal transferred but are all specialized cell junctions to convey information between cells. Across all synapses, this information-sharing capacity is supported by adhesion complexes, thereby focusing signaling, secretion and internalization at the point of cell contact (Dustin and Choudhuri, 2016; Hogg et al., 2011; Park and Goda, 2016). Likewise, we showed that adhesion molecules accumulate at the contact site of pDC/infected cell, and are required for pDC IFN response. Moreover, identical to the immunological synapse, the $\alpha_L\beta_2$ integrin complex is present on the signal recipient cells (pDCs *vs* T cells) and ICAM-1 on the signal delivering cells (infected cells *vs* antigen presenting cells) (Dustin and Choudhuri, 2016). Again like all synapses, the actin network

(and regulators) polarizes at contact and acts as a functional structuring platform. Analogous to the neurological synapse, the mechanism of pDC activation involved a secreted activating signal. In accordance with the transfer of PAMPs *via* vesicles and the endolysosomal localization of the sensor (*i.e.*, TLR7), endocytosis components polarize at contacts. Cell polarity of vesicular trafficking is a hallmark of other synapses, primarily defined for secretory pathways*, e.g.,* local secretion of synaptic vesicles or lytic granules at the neurological and immunological "lytic/NK" synapses, respectively. Additionally, the endocytosis machinery also polarizes at the level of the immunological synapse and regulates T cell activation *via* the internalization and recycling of the T cell receptor (TCR) (Compeer et al., 2018; Das et al., 2004). Importantly, the feed-forward regulation by TLR7-induced signaling is reminiscent of the stabilization of the cell polarity and contact described for immunological and neurological synapses, referred to as inside-out signaling and induced by the response/activation in recipient cells (Dustin and Choudhuri, 2016; Hogg et al., 2011). For example, T-cell receptor engagement at the immunological synapse reinforces cell adhesion by the activation of integrin ectodomain (Dustin and Choudhuri, 2016; Hogg et al., 2011). Therefore, the interferogenic synapse presents hallmarks of other synapses, while being deployed to achieve a distinct cellular response, the IFN response, thus representing a previously unappreciated type of synapse.

Scanning function of pDCs regulated by a TLR7-centered feed-forward signaling.

We propose that the immune surveillance by pDCs involves a scanning function by physical cell contacts (**Figure S8**). In this 'scanning' model, a pDC encounters a cell and initially establishes a transient contact. When the cell is not infected (*i.e.,* in the absence of transfer of PAMPs), the non-activated pDC resumes its motion. By contrast, when a pDC encounters an infected cell, PAMP transfer during the initial contact activates TLR7 in the pDC. In turn,

TLR7-mediated signaling potentiates the structural reorganization at the contact site. These molecular rearrangements include polarized endocytosis components, which can facilitate the subsequent transfer of PAMPs to pDCs and further strengthen TLR7 activation. TLR7-induced signaling primes the establishment of sustained pDC/infected cell contact, which in turn further promotes TLR7 activation, leading to a feed-forward regulatory loop culminating in sustained contacts as well as robust and localized IFN production. As such, the sensing mechanism by pDCs can be seen as a "relay switch": a relatively small initial 'PAMP current' leads to a 'high amperage' flow of PAMPs, *via* a functional platform for efficient PAMP transfer at the contact sites leading to a potent pDC-mediated antiviral response.

TLR7-induced signaling is expected to induce a bifurcated signaling: the transcriptional activators IRF7 and nuclear factor-κB (NF-kB), respectively leading to type I/III IFNs and other inflammatory cytokine response. One might hypothesize that the autocrine/paracrine action of IFNs (and/or subsequently induced-ISGs or other cytokines) could potentiate the interferogenic synapse. Alternatively, the signaling downstream of TLR7, including the phosphorylation cascade might directly reinforce cell contact/polarity (Olayioye et al., 2013; Park et al., 2009; Saitoh et al., 2017).

Local response to viral infection by pDCs.

Systemic and massive productions of IFNs and other inflammatory cytokines are known to be detrimental to the host, as they correlate with systemic homeostatic dysfunction, including tissue damage *e.g.,* increased vascular permeability in the context of DENV (Costa et al., 2013). Here we uncovered that the organization of a functional territory in pDCs at the contact site with infected cells is required for IFN-I production, thus implying that this antiviral response is confined to the proximity of infected cells. This is reminiscent of previous reports showing a pivotal *in vivo* antiviral regulation by early pDC response, despite

undetectable or very transient/limited pDC-derived IFN-I at systemic levels (Swiecki et al., 2010; Webster et al., 2018), thus positioning pDC IFN-I secretion as a response likely confined to the infected site. Therefore, the cell contact-dependent robust pDC response could have evolved in favor of the host fitness to locally respond at the infected sites, and thereby to thwart the otherwise harmful systemic IFN and inflammatory responses.

Albeit not universal, the requirement for cell contact with infected cells is increasingly recognized for pDC activation by a large spectrum of genetically divergent viruses (Webster et al., 2016). It is therefore likely that the interferogenic synapse that we describe here for pDC response to DENV, ZIKV and HCV *via* distinct PAMP-carriers, is also at play for pDC activation by other viruses. Additionally, pDCs can participate in the priming of both immunogenic and tolerogenic adaptive immunity, being also increasingly recognized as pivotal mediators in pathogenesis of autoimmune diseases and cancers (Swiecki and Colonna, 2015). It is possible that the interferogenic synapse is of importance for pDC-mediated sensing in these other contexts.

Acknowledgements

We thank A. D. Davidson (University of Bristol, UK) for the molecular clone NGC, A. Kohn (MRC-University of Glasgow Centre for Virus Research, UK) and R. Freitas de Oliveira Franca (FIOCRUZ, Recife, Brazil) for clinical isolate ZIKV Brazil (PE243_KX197192), the European Virus Archive for H/PF, C. Rice (Rockeffeler University, New York, NY) for the anti-HCV NS5A, P. Despres (PIMIT, Université de La Réunion-INSERM France) for providing the anti-DENV E, F.V. Chisari (Scripps Research Institute, La Jolla, CA) for the Huh7.5.1 cells and V. Lotteau (CIRI, Lyon, France) for Influenza A Virus. We are grateful to Y. Jaillais, H Paidassi, T. Walzer, S. Munoz-Gonzalez for critical reading of the manuscript, and to our colleagues for encouragement and help. The PLATIM platform of SFR Biosciences Lyon-Gerland (UMS3444/US8) for imaging analysis and technical assistance. We acknowledge the contribution of the EFS Confluence-Lyon. This work was supported by grants from the 'Agence Nationale pour la Recherche' (ANR-JCJC-EXAMIN), the 'Agence Nationale pour la Recherche contre le SIDA et les Hépatites Virales' (ANRS-AO 2017-01), the 'Fondation pour le recherche médicale' (DBI20141231313 DREUX Bioinfo 2014) and LabEx Ecofect Grant ANR-11-LABX-0048. SA's PhD fellowship was sponsored by French ministry and Ligue contre le cancer. The post-doc fellowship for BW and DC were sponsored by EMBO and ANRS, respectively.

Author Contributions

Conceived and designed the experiments: SA, SC, DC, LS, BW, MD. Performed the experiments: SA, SC, DC, ED, LS. Analyzed the data: SA, SC, DC, ED, LS, OA, BW, MD. Wrote the paper: SA, SC, MD.

Declaration of Interests

The authors declare no competing interests. The funders had no role in study design, data collection and analysis, decision to publish, or preparation of the manuscript.

References

Bruni, D., Chazal, M., Sinigaglia, L., Chauveau, L., Schwartz, O., Despres, P., and Jouvenet, N. (2015). Viral entry route determines how human plasmacytoid dendritic cells produce type I interferons. Sci Signal *8*, ra25.

Compeer, E.B., Kraus, F., Ecker, M., Redpath, G., Amiezer, M., Rother, N., Nicovich, P.R., Kapoor-Kaushik, N., Deng, Q., Samson, G.P.B.*, et al.* (2018). A mobile endocytic network connects clathrin-independent receptor endocytosis to recycling and promotes T cell activation. Nat Commun *9*, 1597.

Costa, V.V., Fagundes, C.T., da Gloria de Souza, D., and Teixeira, M.M. (2013). Inflammatory and Innate Immune Responses in Dengue Infection: Protection versus Disease Induction. Am J Pathol.

Das, V., Nal, B., Dujeancourt, A., Thoulouze, M.I., Galli, T., Roux, P., Dautry-Varsat, A., and Alcover, A. (2004). Activation-induced polarized recycling targets T cell antigen receptors to the immunological synapse; involvement of SNARE complexes. Immunity *20*, 577-588.

de Chassey, B., Aublin-Gex, A., Ruggieri, A., Meyniel-Schicklin, L., Pradezynski, F., Davoust, N., Chantier, T., Tafforeau, L., Mangeot, P.E., Ciancia, C.*, et al.* (2013). The interactomes of influenza virus NS1 and NS2 proteins identify new host factors and provide insights for ADAR1 playing a supportive role in virus replication. PLoS Pathog *9*, e1003440.

Decembre, E., Assil, S., Hillaire, M.L., Dejnirattisai, W., Mongkolsapaya, J., Screaton, G.R., Davidson, A.D., and Dreux, M. (2014). Sensing of immature particles produced by dengue virus infected cells induces an antiviral response by plasmacytoid dendritic cells. PLoS Pathog *10*, e1004434.

DeMali, K.A., Barlow, C.A., and Burridge, K. (2002). Recruitment of the Arp2/3 complex to vinculin: coupling membrane protrusion to matrix adhesion. The Journal of cell biology *159*, 881-891.

DeMali, K.A., Sun, X., and Bui, G.A. (2014). Force transmission at cell-cell and cell-matrix adhesions. Biochemistry *53*, 7706-7717.

Donald, C.L., Brennan, B., Cumberworth, S.L., Rezelj, V.V., Clark, J.J., Cordeiro, M.T., Freitas de Oliveira Franca, R., Pena, L.J., Wilkie, G.S., Da Silva Filipe, A.*, et al.* (2016). Full Genome Sequence and sfRNA Interferon Antagonist Activity of Zika Virus from Recife, Brazil. PLoS Negl Trop Dis *10*, e0005048.

Doughman, R.L., Firestone, A.J., and Anderson, R.A. (2003). Phosphatidylinositol phosphate kinases put PI4,5P(2) in its place. J Membr Biol *194*, 77-89.

Dreux, M., Garaigorta, U., Boyd, B., Decembre, E., Chung, J., Whitten-Bauer, C., Wieland, S., and Chisari, F.V. (2012). Short-range exosomal transfer of viral RNA from infected cells to plasmacytoid dendritic cells triggers innate immunity. Cell host & microbe *12*, 558-570.

Dreux, M., Gastaminza, P., Wieland, S.F., and Chisari, F.V. (2009). The autophagy machinery is required to initiate hepatitis C virus replication. Proceedings of the National Academy of Sciences of the United States of America *106*, 14046-14051.
Dustin, M.L., and Choudhuri, K. (2016). Signaling and Polarized Communication Across the T Cell Immunological Synapse. Annu Rev Cell Dev Biol *32*, 303-325.
Feng, Z., Li, Y., McKnight, K.L., Hensley, L., Lanford, R.E., Walker, C.M., and Lemon, S.M. (2014). Human pDCs preferentially sense enveloped hepatitis A virions. J Clin Invest.
Garcia-Nicolas, O., Auray, G., Sautter, C.A., Rappe, J.C., McCullough, K.C., Ruggli, N., and Summerfield, A. (2016). Sensing of Porcine Reproductive and Respiratory Syndrome Virus-Infected Macrophages by Plasmacytoid Dendritic Cells. Front Microbiol *7*, 771.
Garcia-Sastre, A. (2017). Ten Strategies of Interferon Evasion by Viruses. Cell host & microbe *22*, 176-184.
Higgs, H.N., and Pollard, T.D. (2000). Activation by Cdc42 and PIP(2) of Wiskott-Aldrich syndrome protein (WASp) stimulates actin nucleation by Arp2/3 complex. The Journal of cell biology *150*, 1311-1320.
Hoffmann, H.H., Schneider, W.M., and Rice, C.M. (2015). Interferons and viruses: an evolutionary arms race of molecular interactions. Trends Immunol *36*, 124-138.
Hogg, N., Patzak, I., and Willenbrock, F. (2011). The insider's guide to leukocyte integrin signalling and function. Nat Rev Immunol *11*, 416-426.
Jost, M., Simpson, F., Kavran, J.M., Lemmon, M.A., and Schmid, S.L. (1998). Phosphatidylinositol-4,5-bisphosphate is required for endocytic coated vesicle formation. Curr Biol *8*, 1399-1402.
Kato, T., Date, T., Miyamoto, M., Furusaka, A., Tokushige, K., Mizokami, M., and Wakita, T. (2003). Efficient replication of the genotype 2a hepatitis C virus subgenomic replicon. Gastroenterology *125*, 1808-1817.
Kroschewski, H., Lim, S.P., Butcher, R.E., Yap, T.L., Lescar, J., Wright, P.J., Vasudevan, S.G., and Davidson, A.D. (2008). Mutagenesis of the dengue virus type 2 NS5 methyltransferase domain. The Journal of biological chemistry *283*, 19410-19421.
Lepelley, A., Louis, S., Sourisseau, M., Law, H.K., Pothlichet, J., Schilte, C., Chaperot, L., Plumas, J., Randall, R.E., Si-Tahar, M.*, et al.* (2011). Innate sensing of HIV-infected cells. PLoS Pathog *7*, e1001284.
Martel, V., Racaud-Sultan, C., Dupe, S., Marie, C., Paulhe, F., Galmiche, A., Block, M.R., and Albiges-Rizo, C. (2001). Conformation, localization, and integrin binding of talin depend on its interaction with phosphoinositides. The Journal of biological chemistry *276*, 21217-21227.
Martina, B.E., Koraka, P., and Osterhaus, A.D. (2009). Dengue virus pathogenesis: an integrated view. Clin Microbiol Rev *22*, 564-581.
Meertens, L., Carnec, X., Lecoin, M.P., Ramdasi, R., Guivel-Benhassine, F., Lew, E., Lemke, G., Schwartz, O., and Amara, A. (2012). The TIM and TAM families of phosphatidylserine receptors mediate dengue virus entry. Cell host & microbe *12*, 544-557.
Miner, J.J., and Diamond, M.S. (2017). Zika Virus Pathogenesis and Tissue Tropism. Cell host & microbe *21*, 134-142.
Nordenfelt, P., Elliott, H.L., and Springer, T.A. (2016). Coordinated integrin activation by actin-dependent force during T-cell migration. Nat Commun *7*, 13119.
Olayioye, M.A., Barisic, S., and Hausser, A. (2013). Multi-level control of actin dynamics by protein kinase D. Cell Signal *25*, 1739-1747.
Park, J.E., Kim, Y.I., and Yi, A.K. (2009). Protein kinase D1 is essential for MyD88-dependent TLR signaling pathway. J Immunol *182*, 6316-6327.

Park, Y.K., and Goda, Y. (2016). Integrins in synapse regulation. Nat Rev Neurosci *17*, 745-756.
Posor, Y., Eichhorn-Grunig, M., and Haucke, V. (2015). Phosphoinositides in endocytosis. Biochim Biophys Acta *1851*, 794-804.
Rohatgi, R., Ma, L., Miki, H., Lopez, M., Kirchhausen, T., Takenawa, T., and Kirschner, M.W. (1999). The interaction between N-WASP and the Arp2/3 complex links Cdc42-dependent signals to actin assembly. Cell *97*, 221-231.
Rothlein, R., Dustin, M.L., Marlin, S.D., and Springer, T.A. (1986). A human intercellular adhesion molecule (ICAM-1) distinct from LFA-1. J Immunol *137*, 1270-1274.
Rotty, J.D., Wu, C., and Bear, J.E. (2013). New insights into the regulation and cellular functions of the ARP2/3 complex. Nat Rev Mol Cell Biol *14*, 7-12.
Rozelle, A.L., Machesky, L.M., Yamamoto, M., Driessens, M.H., Insall, R.H., Roth, M.G., Luby-Phelps, K., Marriott, G., Hall, A., and Yin, H.L. (2000). Phosphatidylinositol 4,5-bisphosphate induces actin-based movement of raft-enriched vesicles through WASP-Arp2/3. Curr Biol *10*, 311-320.
Saitoh, S.I., Abe, F., Kanno, A., Tanimura, N., Mori Saitoh, Y., Fukui, R., Shibata, T., Sato, K., Ichinohe, T., Hayashi, M.*, et al.* (2017). TLR7 mediated viral recognition results in focal type I interferon secretion by dendritic cells. Nat Commun *8*, 1592.
Salas, A., Shimaoka, M., Phan, U., Kim, M., and Springer, T.A. (2006). Transition from rolling to firm adhesion can be mimicked by extension of integrin alphaLbeta2 in an intermediate affinity state. The Journal of biological chemistry *281*, 10876-10882.
Sen, M., Koksal, A.C., Yuki, K., Wang, J., and Springer, T.A. (2018). Ligand and cation-induced structural alterations of the leukocyte integrin LFA-1. The Journal of biological chemistry.
Shimaoka, M., Xiao, T., Liu, J.H., Yang, Y., Dong, Y., Jun, C.D., McCormack, A., Zhang, R., Joachimiak, A., Takagi, J.*, et al.* (2003). Structures of the alpha L I domain and its complex with ICAM-1 reveal a shape-shifting pathway for integrin regulation. Cell *112*, 99-111.
Snell, L.M., McGaha, T.L., and Brooks, D.G. (2017). Type I Interferon in Chronic Virus Infection and Cancer. Trends Immunol *38*, 542-557.
Sozzani, S., Vermi, W., Del Prete, A., and Facchetti, F. (2010). Trafficking properties of plasmacytoid dendritic cells in health and disease. Trends Immunol *31*, 270-277.
Swiecki, M., and Colonna, M. (2015). The multifaceted biology of plasmacytoid dendritic cells. Nat Rev Immunol *15*, 471-485.
Swiecki, M., Gilfillan, S., Vermi, W., Wang, Y., and Colonna, M. (2010). Plasmacytoid dendritic cell ablation impacts early interferon responses and antiviral NK and CD8(+) T cell accrual. Immunity *33*, 955-966.
Takahashi, K., Asabe, S., Wieland, S., Garaigorta, U., Gastaminza, P., Isogawa, M., and Chisari, F.V. (2010). Plasmacytoid dendritic cells sense hepatitis C virus-infected cells, produce interferon, and inhibit infection. Proceedings of the National Academy of Sciences of the United States of America *107*, 7431-7436.
Vicente-Manzanares, M., Choi, C.K., and Horwitz, A.R. (2009). Integrins in cell migration--the actin connection. Journal of cell science *122*, 199-206.
Webster, B., Assil, S., and Dreux, M. (2016). Cell-Cell Sensing of Viral Infection by Plasmacytoid Dendritic Cells. Journal of virology *90*, 10050-10053.
Webster, B., Werneke, S.W., Zafirova, B., This, S., Coleon, S., Decembre, E., Paidassi, H., Bouvier, I., Joubert, P.E., Duffy, D.*, et al.* (2018). Plasmacytoid dendritic cells control dengue and Chikungunya virus infections via IRF7-regulated interferon responses. Elife *7*.

Wieland, S.F., Takahashi, K., Boyd, B., Whitten-Bauer, C., Ngo, N., de la Torre, J.C., and Chisari, F.V. (2014). Human plasmacytoid dendritic cells sense lymphocytic choriomeningitis virus-infected cells in vitro. Journal of virology *88*, 752-757.
Zhong, J., Gastaminza, P., Cheng, G., Kapadia, S., Kato, T., Burton, D.R., Wieland, S.F., Uprichard, S.L., Wakita, T., and Chisari, F.V. (2005). Robust hepatitis C virus infection in vitro. Proceedings of the National Academy of Sciences of the United States of America *102*, 9294-9299.

Figure Legends

Figure 1. Identification of adhesion molecules involved for pDC-mediated antiviral response against DENV. (A) Quantification of IFNα in supernatants of pDCs cocultured with DENV infected Huh-7.5.1 cells that were treated or not with blocking antibodies against L-selectin, E-cadherin, α_L integrin or ICAM-1 at 10 μg/ml. The intracellular and extracellular viral RNA levels and extracellular infectious virus production by DENV infected cells treated with blocking antibodies were analyzed in absence of pDC, but with treatment conditions similar to the analysis of IFNα production in cocultures (*i.e.,* incubation time and concentration). Results are expressed as percentages relative to untreated cells; mean±SD; 4-7 independent experiments. The statistically significances reflected by p-values are indicated in the table; not significant (NS; $p \geq 0.05$). **(B)** Quantification of IFNβ and type III IFNs (IL-29/28A/28B) in supernatants of DENV infected cell/pDC cocultures treated, or not, with blocking anti-α_L integrin as in **A**. Results expressed as pg/ml; mean±SD. **(C)** Quantification of conjugates between pDCs and DENV infected cells by Image Stream X technology, as exemplified in **Figure S1D**. Celltracer violet stained-pDCs were cocultured with GFP^+ Huh7.5.1 infected cells for 4-5 hour incubation in presence or not of anti-α_L integrin or anti-ICAM-1. Results of 5 independent experiments for each graph expressed as percentage of conjugates; mean±SD; n=10 000 events per condition. **(D-E)** FACS analysis of viral transmission from GFP^- DENV infected cells to GFP^+ uninfected cells cocultured with/without pDCs for 48 hours and in presence of anti-α_L integrin (10 μg/mL). (**D**) Dot plots of a representative experiment. (**E**) Results expressed as the percentage of cells positive for dsRNA (a marker of viral replication) in the GFP^+ and GFP^- cell populations, mean±SD; 5 independent experiments; p-value are indicated in green and grey for GFP^+ and GFP^- cells, respectively. **(F)** Quantification of extracellular infectious virus production harvested after 48

hour-coculture, as in **D-E** and expressed as foci forming unit (ffu) per mL, mean±SD. **(G-H)** Down-regulation of ICAM-1 expression in Huh7.5.1 cells obtained by transduction using shRNA-expressing lentiviral vectors. **(G)** FACS analysis of ICAM-1 surface expression: representative histogram and quantifications expressed as fold-increases of geomean relative to unstained cells; n=4 independent experiments. **(H)** Quantification of IFNα in supernatants of pDCs cocultured with DENV infected Huh-7.5.1 cells down-regulated or not for ICAM-1 expression, as in **G.** The intra/extracellular viral RNA levels and infectivity were analyzed in the absence of pDC. Error bar represents mean±SD; n=4 independent experiments.

Figure 2. Accumulation of α_L integrin and its ligand ICAM-1 at the contact. (**A-C**) Confocal microscopy imaging of immunostained α_L integrin (green) and CD123 (purple) in co-cultures of pDCs (DiI staining prior to coculture; red; marked by *) and DENV Huh7.5.1 infected cells (#) for 4-5 hour-incubation; nuclei stained with Hoechst (blue). **(A)** Detection of α_L integrin, CD123, DiI and Hoechst projected on the phase contrast imaging. **(B)** Magnification of two consecutive Z-stacks of yellow-boxed pDC shown in **A.** (**C**) Quantification of the frequency of pDCs with accumulation of α_L integrin or CD123 at contact. Results of 3 independent experiments are expressed as the percentage of total number of analyzed pDCs in contact with infected cells; mean±SD; n=39 analyzed contacts; p-value as indicated. (**D-F**) Confocal microscopy imaging of immunostained open/high-affinity conformation of $\alpha_L\beta_2$ integrin complex (detection of the exposure of m24 epitope in β_2 I domain) in co-cultures of pDCs (DiI stained; *) and DENV infected cells (#), 4-5 hour-incubation; nuclei (Hoechst). Detection of the open/high-affinity conformation of $\alpha_L\beta_2$ integrin complex projected on the phase contrast imaging (**D**), magnification of two consecutive Z-stacks of yellow-boxed pDC shown (**E**) and 3D-reconstruction of consecutive Z-stacks of blue-boxed pDC (**F**). (**G-H**) Confocal microscopy imaging of immunostained α_L

integrin (**G**) and the high-affinity conformation of $\alpha_L\beta_2$ integrin complex (**H**) in pDCs in absence of contact, displayed as in **D-E**. **(I)** Quantification of the frequency of α_L integrin with accumulation or diffuse localization around pDCs. Results of 3 independent experiments are expressed as in the percentage of total number of analyzed pDCs in contact with infected cells *versus* in absence of contact; mean±SD; n>37 analyzed contacts. (**J-L)** Confocal microscopy imaging of immunostained α_L integrin and ICAM-1 in co-cultures of pDCs (CTV stained) and DENV infected cells, 4-5 hour-incubation. Staining of α_L integrin/ICAM-1 projected on the phase contrast imaging (**J**) and magnification of two consecutive Z-stacks of yellow-boxed pDC shown (**K**) and 3D-reconstruction of consecutive Z-stacks of blue-boxed contacts, with colocalized signal in white (**L**).

Figure 3. Inhibition of α_L integrin and ICAM-1 prevents pDC IFNα production induced by coculture with cells infected by distinct viruses. (A) Quantification of IFNα in supernatants of pDCs cocultured with HCV infected Huh7.5.1c2 cells that were treated or not with blocking antibodies against α_L integrin or ICAM-1. The intra/extracellular viral RNA levels and infectious virus production by infected cells treated with blocking antibodies were analyzed in absence of pDCs. Results and statistical significances are presented as in **Figure 1A**; mean±SD; n=4-7 independent experiments. **(B)** Quantification of conjugate between pDCs and HCV Huh7.5.1c2 infected cells in presence or not of anti-α_L integrin or -ICAM-1; 5 independent experiments; expressed as in **Figure 1C**. **(C)** Quantification of IFNα in supernatants of pDCs stimulated by cell-free influenza virus and treated with blocking antibodies as in **A**; mean±SD, n=3-4 independent experiments. **(D)** Quantification of IFNα in supernatants of pDCs cocultured with Huh-7.5.1 cells infected by the epidemic ZIKV strains [*i.e.,* clinical isolated from patients in Brazil and French Polynesia; H/PF] when cells were in physical contact [coculture], separated by the permeable membrane of transwell [TW], or

treated with supernatants from ZIKV infected cells [SN] or imiquimod at 20 μM [IMQ], as positive control. Mean±SD; n=4-7 experiments; non detectable (arrays). **(E-G)** Quantification of IFNα in supernatants of pDCs cocultured with ZIKV infected Huh-7.5.1 cells treated or not with anti-α_L integrin or anti-ICAM-1 blocking antibodies and parallel analysis of intra/extracellular viral RNA levels and infectivity in absence of pDC, as in **A**. Mean±SD; n=4-5 (E) and n=3 (F-G) independent experiments. **(I-J)** FACS analysis of viral spread from GFP^- ZIKV infected cells to GFP^+ uninfected cells prior to coculture (**I**) and quantification of infectious virus production (**J**) in presence of pDCs and blocking antibody, as indicated. Experiments performed and expressed as in **Figure 1E-F**; 5 independent experiments.

Figure 4. Actin network regulators polarize at the contact and an intact actin network is required for pDC response. (**A-L**) Confocal microscopy imaging of immunostained $PI(4,5)P_2$ and PIP5KIα in 4-5 hour cocultures of pDCs (DiI stained) and DENV (**A-C**), HCV infected cells (**E-G**) and HCV replicating (rep) Huh7.5.1c2 cells (**I-K**), nuclei (Hoechst). Imaging of $PI(4,5)P_2$ and PIP5KIα projected on the phase contrast (**A, E, I**), confocal stacks of magnification of yellow-boxed pDC (**B, F, J**) and 3D-reconstruction of consecutive Z-stacks with colocalization of $PI(4,5)P_2$/PIP5KIα in white (**C, G, K**). (**D, H, L**) Quantification of the phenotype of $PI(4,5)P_2$/PIP5KIα co-clustering as indicated (*i.e.,* co-cluster at the contacts, outside the contact or no co-cluster) in pDCs cocultured with infected cells and treated with inhibitors of Arp 2/3 complex (CK-666; 60 μM) or actin polymerization (Latrunculin B, Lat B; 1 μM). Results of 3 independent experiments (D; n>53, H; n>40, L; n>21 analyzed contacts per condition) are expressed as the percentage of total number of analyzed pDCs in contact; mean±SD; p-value as indicated. **(M-P).** Quantification of IFNα in supernatants of pDCs cocultured with DENV infected (**M**), HCV infected (**N**) or HCV rep Huh7.5.1c2 cells (**O**) treated or not with inhibitor of Arp 2/3 complex (CK-666). The levels of

intra/extracellular viral RNAs by infected/replicating cells treated with inhibitors were analyzed in absence of pDC. Results are expressed as percentages relative to untreated cells; mean±SD; n=4 (M-N) and n=3 (0) independent experiments; p-value as indicated. (**P**) Quantification of IFNα in supernatants of pDCs stimulated by cell-free influenza virus and treated or not with inhibitor of Arp 2/3 complex, presented as in **Figure 3C**; mean±SD; n=4. **(Q-R)** Quantification of pDC/infected cell conjugates by Image Stream X technology. Celltrace Violet stained-pDC cocultured with GFP^+ DENV or HCV-infected cells for 4-5 hours treated or not with Arp 2/3 complex inhibitor, as in **M-O**. Results of 4 (Q) and 5 (R) independent experiments are expressed as percentage of conjugates; mean±SD; n=10 000 events per condition.

Figure 5. Polarization of endocytosis machinery components at the cell contact. (A-F) Confocal microscopy imaging of immunostained $PI(4,5)P_2$ and EEA1 in cocultures of pDCs and DENV infected cells for 4-5 hours (**A-C**) and HCV (rep) replicating cells for 7-8 hours (**D-F**); nuclei (Hoechst). Representative detection of $PI(4,5)P_2$ and EEA1 projected on the phase contrast imaging (**A, D**), two successive confocal stacks with magnified yellow-boxed pDC (**B, E**) and 3D-reconstruction of consecutive Z-stacks of the blue-boxed view, $PI(4,5)P_2$/EEA1 colocalization in white (**C, F**). **(G-I)** Confocal microscopy imaging of immunostained clathrin and actin co-clustering in 4-5 hour cocultures of pDC/HCV infected cells, displayed as in A-C. **(J-L)** Quantification of EEA1/$PI(4,5)P_2$ (**J-K**) and clathrin/actin co-clustering (**G**) in coculture treated with inhibitors of Arp2/3 or actin polymerization, as in **Figure 4D**. Results of 3 independent experiments are expressed as in **Figure 4D**; mean±SD; n>43 (J); n>50 (K) n>40 (L) analyzed contacts per condition.

Figure 6. Establishment of sustained contact of pDCs with infected cells regulated by α_L integrin and TLR7-induced signaling. (A) Quantification of conjugates of pDCs with cells infected by DENV or HCV *versus* uninfected cells by Image Stream X technology. Results of 6 independent experiments are expressed as percentage of conjugates; n=10 000 events per condition. (**B-I**) Quantification of the duration of cell contacts between pDCs and DENV infected cells (**B, D, F, H**), HCV replicating (rep) cells (**C, G**), uninfected (cont cells) (**B, C, E, F, G, I**) determined by live-imaging with spinning-disc confocal microscopy (see details in STAR Methods). As indicated, the cocultures were treated with TLR7 inhibitor (IRS661; 0.35 μM) (**B, F**), anti-α_L integrin blocking antibody (10 μg/ml) (**D, H**) or TLR7 agonist (IMQ; 20 μM) (**E, I**). Confocal Z-stacks of cocultures of DiI stained-pDCs and GFP^+ infected or uninfected cells are acquired every 5 minutes. The cell contact is defined as DiI signal (pDCs) apposed/merged with GFP signal (HCV/DENV/cont cells), as shown on **Figure S6A**. The results of 3-4 independent experiments are presented by violin plots with dots representing the durations of the individual recorded contacts in each indicated experimental condition (**B-E**) and displayed as percentages of contacts in the indicated time interval relative to the total number of examined pDC/infected cell contacts (**F-I**).

Figure 7. TLR7-mediated pDC activation potentiates cell polarity at the contact. (A-B) Quantification of the α_L integrin accumulation and α_L integrin/ICAM-1 co-accumulation at the contact between pDCs and DENV (**A**) or HCV (**B**) infected cells *versus* uninfected (cont) cells, analyzed as in **Figure 2J-L.** Results are expressed as the percentage of indicated phenotype relative to the total number of analyzed contacts; 4 (A; n>62 analyzed contacts per condition) and 3 (B; n>46) independent experiments; mean±SD. **(C-L)** Quantification of the co-clustering of $PI(4,5)P_2$/PIP5KIα (**C, F, I**), $PI(4,5)P_2$/EEA1 (**D, G**), clathrin/actin (**J-L**), α_L integrin/clathrin (**E**) and high-affinity conformation $\alpha_L\beta_2$ integrin complex/EEA1 (**H**), as

shown in **Figure 4A-L, 5, S5, S7** in cocultures of pDCs with uninfected (cont) cells, or with cells infected by DENV, ZIKV or HCV or HCV rep cells, in the presence or not of TLR7 inhibitor (IRS661; 0.35 μM). Results are expressed as the percentage of the indicated phenotype relative to the total number of analyzed pDCs in contact with infected cells; 3 (D, F, G, I, L), 7 (J), 4 (C, E, H, K) independent experiments; mean±SD.

STAR Methods

KEY RESOURCES TABLE

CONTACT FOR REAGENT AND RESOURCE SHARING

Further information and requests for resources and reagents should be directed to and will be fulfilled by the Lead Contact, Dr. Marlène Dreux (marlene.dreux@ens-lyon.fr).

EXPERIMENTAL MODEL AND SUBJECT DETAILS

Cell lines and primary cell cultures.

Huh7.5.1, Huh-7.5.1c2 cells and Huh-7.5.1c2 cells (male) that harbor the JFH-1 subgenomic replicon (HCV rep cells) (Kato et al., 2003) were maintained in Dulbecco's modified Eagle medium (DMEM) (Life Technologies) supplemented with 10% FBS, 100 units (U)/ml penicillin, 100 mg/ml streptomycin, 2 mM L-glutamine and non-essential amino acids (Life Technologies) at 37°C/5% CO_2 (Decembre et al., 2014; Dreux et al., 2012).

The pDCs were isolated from blood or cytapheresis units from healthy adult human volunteers which was obtained from the 'Etablissement Français du Sang' (EFS; Auvergne Rhône Alpes, France) under the convention EFS 16–2066 and according to procedures approved by the EFS committee. Informed consent was obtained from all subjects in accordance with the Declaration of Helsinki. Information on sex and age was not available for all subjects, however was not relevant for the purpose of the study, since we previously showed that pDC responses are within the range for all donors (Decembre et al., 2014). PBMCs were isolated using Ficoll-Hypaque density centrifugation and pDCs were positively selected from PBMCs using BDCA-4-magnetic beads (MACS Miltenyi Biotec), as previously described (Decembre et al., 2014; Dreux et al., 2012). The typical yields of PBMCs and pDCs

were $800x10^6$ and $2x10^6$ cells, respectively, with a typical purity of >95% pDCs. Isolated pDCs were maintained in RPMI 1640 medium (Life Technologies) supplemented with 10% FBS, 10 mM HEPES, 100 units/ml penicillin, 100 mg/ml streptomycin, 2 mM L-glutamine, non-essential amino acids and 1 mM sodium pyruvate at 37°C/5% CO_2.

The down regulation of ICAM-1 in huh7.5.1 cells was achieved using lentivirus-based vector expressing shRNA against ICAM-1 (TRCN0000372477, target sequence: GCCCGAGCTCAAGTGTCTAAA, Sigma-Aldrich), produced using 293T cells (female), as we previously described (Dreux et al., 2012). Cells were transduced 4 days prior to infection by DENV for 48 hours and followed by coculture with pDCs.

Preparation of viral stocks and infections.

Viral stocks of HCV JFH1 strain (Zhong et al., 2005) and the prototypic DENV-2 strain New Guinea C (NGC) (AF038403) (Kroschewski et al., 2008) were produced as previously described (Decembre et al., 2014; Dreux et al., 2012). The clinical isolate of epidemic strains of ZIKV including from Brazil (PE243_KX197192) (Donald et al., 2016) and H/PF from French Polynesia (H/PF/2013_KJ776791.1) obtained from the European Virus Archive (EVA) were amplified using Vero cells (female). Huh7.5.1 cells were infected by DENV or ZIKV (MOI of 1) and Huh-7.5.1c2 cells by the cell-culture adapted HCV JFH-1 virus (MOI of 1) (Decembre et al., 2014; Dreux et al., 2012) 48 hours prior to co-culture with isolated pDCs.

Viral stocks of Influenza A Virus (FluAV, H1N1/New Caledonia/2006) were produced as previously described (de Chassey et al., 2013) and kindly provided by Dr V. Lotteau (CIRI, Lyon, France).

Reagents.

The antibodies used for immunostaining were mouse anti-DENV E glycoprotein (hybridoma, clone 3H5 and 4G2) kindly provided by P. Despres (PIMIT, Université de La Réunion-INSERM France); mouse anti-HCV NS5A (clone 9E10) kindly provided by C. Rice (Rockefeller University, New York, US); mouse anti-dsRNA (clone J2; Scicons); mouse anti-integrin α_L subunit (clone 38; LSBio); mouse anti-integrin β_2 I-like domain, *i.e* high-affinity conformation - m24 epitope (Biolegend); mouse anti-ICAM-1 (clone LB-2; BD Pharmingen); mouse anti-E-Cadherin (SHE78-7; Life Technologies); mouse anti-L-selectin/CD62L (unconjuguated clone DREG55; Invitrogen and Clone 145/15; Vioblue-conjugated; Miltenyi); mouse anti-actin (clone AC74; Sigma-Aldrich); rabbit anti-protein disulfide isomerase (PDI) (anti-P4HB, HPA018884, Sigma-Aldrich); mouse anti-PI(4,5)P_2 (ab2335, Abcam); goat anti-PIP5KIα (reference C-17/sc-11774, Santa Cruz); rabbit anti-clathrin (ab21679, Abcam); rabbit anti-EEA1 (ALX-210-239, Enzo Life Sciences); pDC specific markers: mouse PE or APC-conjugated anti-CD123 (clone AC145, Miltenyi), mouse APC-conjugated anti-BDCA-2 (AC144; Miltenyi) and Alexa-conjugated secondary antibodies for confocal analysis (Life Technologies) and APC-conjugated secondary antibodies for FACS analysis (Southern Biotech).

The inhibitors used were Latrunculin B (Sigma-Aldrich); Arp2/3 complex inhibitor I (CK-666, Merck Millipore); CDC42 inhibitor (ML141, Sigma-Aldrich); chlorpromazine (CPZ, Sigma-Aldrich), dynasore (Sigma-Aldrich); TLR7 inhibitor IRS661 (5'-TGCTTGCAAGCTTGCAA GCA-3') synthesized on a phosphorothioate backbone (Decembre et al., 2014).

The other reagents were TLR7 agonist (Imiquimod; IMQ; Invivogen); Ficoll-Hypaque (GE Healthcare Life Sciences); Fc Blocking solution (MACS Miltenyi Biotec); ELISA kits (PBL Interferon Source) for the specific detections of IFNα, IFNβ and type III IFNs (including IL-29/28A/28B); 96-Well Optical-Bottom Plates and Nunc UpCell 96F Microwell Plate (Thermo Fisher Scientific); 96-well format transwell chambers separated by a 0.4 mm membrane

(Corning); Vybrant cell-labeling solution (CM-DiI, Life Technologies); Celltrace Violet cell Proliferation kit (Life Technologies); Hoescht and Fc receptor blocking reagent (MACS Miltenyi Biotec); cDNA synthesis and qPCR kits (Life Technologies); poly-L-lysin (P6282, Sigma-Aldrich).

METHOD DETAILS

Immunostaining and FACS analysis.

Surface immunostainings were performed on freshly isolated pDCs, DENV infected and uninfected Huh-7.5.1 cells and cocultured cells that were harvested and resuspended using 0.48 mM EDTA-PBS solution. Surface adhesion molecules were detected by a 30 minute-incubation at 4°C with 5 µg/mL of mouse anti-α_L integrin (clone 38); mouse anti-ICAM-1 (Clone LB-2); mouse anti-E-cadherin (clone SHE78-7); Vioblue-conjugated mouse anti-L-selectin/CD62L (clone 145/15) diluted in staining buffer (PBS - 1% FBS), followed by PBS washes. For α_L integrin, ICAM-1 and E-cadherin detection, cells were incubated for 20 minutes with APC-conjugated-anti-mouse antibody diluted in staining buffer (2 µg/mL) and cells were fixed in PFA4% (20 min, 4°C). Flow cytometric analysis was performed using a BD FACS Canto II, and the data were analyzed with Flow Jo software (Tree Star).

Co-culture experiments.

Unless otherwise indicated, 10^4 pDCs were co-cultured with $2x10^4$ infected cells or uninfected parental cells in a 200 µl final volume in 96-well round-bottom plates incubated at 37 °C/5% CO_2. Eighteen to twenty hours later, cell-culture supernatants were collected and the levels of IFNα and, when indicated, IFNβ and type III IFNs, were measured using a commercially available specific ELISA kit (PBL Interferon Source) following the manufacturer's instructions. To optimize the pDC response to HCV replicating (SGR) cells, $2x10^4$ pDCs

were co-cultured with 10^5 cells for 22-to-24 hours.

Viral spread assay.

5x10e4 GFP+ uninfected cells and 5x10e4 GFP- cells, that were infected by DENV or ZIKV, as indicated, for 48 hours prior to coculture, were cocultured with 2x10e4 pDCs, 48 hour-incubation. When indicated, the cocultures were treated by anti-α_L integrin at 10 µg/mL. The levels of the viral spread from infected cells (GFP-) to uninfected cells (GFP+) during coculture were determined by FACS analysis of the frequency of infected cells in the GFP+ cell population. Similar detection in GFP- populations demonstrated the inhibition of viral replication during coculture. The infected cells were detected by immunostaining of dsRNA, a marker of viral replication. Briefly, after 48 hours of coculture, cells were fixed with 4% PFA, followed by PBS washes and a permeabilization step with 90% methanol/10% PBS for 1 hour-incubation at 20°C. The mouse anti-dsRNA (clone J2; Scicons) was diluted at 1 µg/mL staining buffer (PBS - 1% FBS) and added to the cells for an hour incubation at 4°C. After PBS wash, cells were incubated with anti-mouse IgG2a conjugated with Alexa 647-fluorochrome and diluted staining buffer with 30 minute incubation at 4°C. Flow cytometric analysis was performed using a BD FACS Canto II, and the data were analyzed with Flow Jo software (Tree Star).

Imaging combined with flow cytometry analysis.

Huh 7.5.1c2 cells were transduced with lentiviral based vector pseudotyped with VSV glycoprotein to stably express GFP, as previously described (Decembre et al., 2014; Dreux et al., 2009). Forty-eight hours prior co-culture with pDCs, GFP-expressing Huh 7.5.1c2 cells were infected by HCV or DENV as above-described. After immuno-isolation, pDCs were stained by using Celltrace Violet Cell Proliferation kit (Life Technologies) by 20 minute-

incubation at 37°C in the dark. Labeled pDCs were then spinned down and resuspended into pDC coculture medium. 10^5 GFP-expressing HCV/DENV infected or uninfected cells were co-cultured with 4 x 10^4 pDCs in low-adherence micro-plate designed for cell harvesting by temperature reduction (Nunc UpCell 96F Microwell Plate from Thermo Scientific) for 4-5 hours at 37°C in presence or not of inhibitor, as indicated. The co-cultured cells were detached and harvested by 20 minute-incubation at room temperature. After 2% PFA fixation, cells are washed twice with staining buffer (PBS 2% FBS). Co-cultured cells were analyzed by Image Stream X technology (Amnis) at magnification x40 using IDEAS software. The cell population defined as pDC/HCV-infected or uninfected cell conjugates comprises conjugates of at least one Celltrace Violet (CTV) positive cell and at least one GFP positive cell among the total of CTV positive cells, GFP positive cells and conjugates. The cell populations were sorted by using masks (IDEAS software) to eliminate cells not in focus and/or with saturating fluorescent signal, conjugate population was further selected by with Area dilate IDEAS mask (*i.e.,* double fluorescent signal without overlay) and then sorted based of cell size of the positive cells (*i.e.,* fluorescent signal area). Post-cell sorting, the accuracy of the gated cell populations in regards to the defined criteria was controlled by a visual inspection of the individual pictures in the gated cells population *(***Figure S1D**).

Immunostaining for confocal analysis.

After immuno-isolation, 4 x 10^4 pDCs were stained by using either 0.5 µM Vybrant cell-labeling solution (CM-DiI, Life Technologies) by successive incubations for 10 and 15 minutes at 37°C and 4°C, respectively or Celltrace Violet cell Proliferation kit (Life Technologies) as above-described. Labeled pDCs were washed twice with PBS and then co-cultured with 2 x 10^4 DENV infected Huh7.5.1 cells or HCV infected Huh7.5.1c2 cells at 37°C for 4-5 hours, in a 96-Well Optical-Bottom Plate pre-coated with 8 µg/mL poly-L-lysin

for 30 minutes incubation at 37°C. A longer incubation time (*i.e.,* 7-8 hours) was preferred for analysis of clathrin/actin and EEA1/PI(4,5)P_2 in HCV cells, as a pilot experiment suggested that the polarization of endocytic components is slightly higher at this time point. After 4% PFA fixation and three PBS washes, immunostainings were performed without additional permeabilization step, as previously (Decembre et al., 2014; Meertens et al., 2012). After blocking step (PBS 3% BSA), primary antibody antibodies were diluted in 3% BSA-PBS and added to the cell for one hour incubation at room temperature. Primary antibodies used in this study include mouse anti-actin (20 µg/mL); rabbit anti-PDI (2 µg/mL); mouse anti-PI(4,5)P_2 (20 µg/mL); goat anti-PIPK1α (4 µg/mL); rabbit anti-clathrin (2 µg/mL); rabbit anti-EEA1 (2 µg/mL); mouse anti-ICAM-1 (10 µg/mL); mouse anti-α_L integrin subunit (clone 38 LSBio at 5 µg/mL); mouse anti-integrin β_2 I-like domain, *i.e.,* open/high-affinity conformation of $\alpha_L\beta_2$ integrin complex (Nordenfelt et al., 2016; Salas et al., 2006; Sen et al., 2018) (clone m24 at 5 µg/mL); APC-conjugated mouse anti-CD123 (clone AC145 at 5 µg/mL). After three washes with PBS, cells were incubated with the appropriate anti-mouse, rabbit or goat antibody [conjugated with Alexa 488-, 555- or 647-fluorochrome] or Alexa-conjugated antibody against specific mouse isotypes [*i.e.,* anti-IgG1 for detection of m24 epitope of □$_L\beta_2$ integrin complex and anti-IgG2a for detection of the integrin α_L subunit] at 2 µg/mL in 3% BSA-PBS and add to the cells along with Hoechst diluted at 1:1000 (Molecular Probes) for 1 hour incubation at room temperature. After three gentle washes with PBS, cells were observed with a Zeiss LSM 710 laser scanning confocal microscope. The quantification of the phenotypes defined to as clusters or co-clusters at the contact, outside contact or no cluster/co-clusters were performed using Image J software package (http://rsb.info.nih.gov/ij); Results were validated in a "double-blind" set-up. IMARIS (Bitplane Inc.) software package with coloc tools was used for the 3D-reconstructions of the consecutive Z-stacks.

Live imaging of coculture.

Huh 7.5.1c2 cells were transduced with lentiviral based vector to stably express GFP and infected, or not, with HCV or DENV 48 hours before co-culture, as above described. GFP-expressing DENV infected cells or HCV replicating cells and corresponding uninfected control (cont) cells were seeded (2 x 10^4 cells per well) in a 96-Well Optical-Bottom Plate pre-coated with poly-L-lysin (30 minutes incubation at 37°C with 8 µg/mL poly-L-lysin). Isolated pDCs were stained with Vybrant cell-labeling solution (CM-DiI, Life Technologies) as above described. When pDCs were added to the seeded infected (or uninfected) cells, the cocultures were imaged every 5 minutes for 10 hours at magnification x10 with a BSL3-based spinning-disc confocal microscope (AxioObserver Z1, Zeiss). The cocultures were maintained at 37°C, 5% CO2 in an incubation chamber throughout the course of the experiments. The analyses of pDC motion (as illustrated in **Figure S6**) were performed using projection of Z-stacks with maximal intensity (*i.e.,* about 3-to-5 selected Z-stacks per fields out of 15 Z-stacks in total). The quantification of the duration of contacts between pDCs and infected cells *versus* uninfected cells were performed using Image J software package (http://rsb.info.nih.gov/ij). The calculations of cell positions for the motion graphs were performed using Trackmate plug-in of Image J software. The representation with violin plots were obtained using R software environment for statistical computing and graphics, version 3.3.2. The results of **Figure S6L-M** were obtained by 10 hour-records in similar condition (37°C, 5% CO2) of the isolated pDCs (stained by CellTracker Red CMTPX fluorescent dye) in absence of other cells. The pDC velocities were determined by using Trackmate plug-in of Image J software.

Analysis of viral RNA levels.

RNAs were isolated from cells or supernatants harvested in guanidinium thiocyanate citrate buffer (GTC) by phenol/chloroform extraction procedure as previously described (Dreux et al., 2012). The efficiency of RNA extraction and reverse transcription-real-time quantitative PCR (RT-qPCR) was controlled by the addition of carrier RNAs encoding Xef1α (xenopus transcription factor 1α) *in vitro* transcripts in supernatants diluted in GTC buffer. DENV, HCV and ZIKV RNA, Xef1α and intracellular glyceraldehyde-3-phosphate dehydrogenase (GAPDH) mRNA levels were determined by RT-qPCR using cDNA synthesis and qPCR kits (Life Technologies) and analyzed using StepOnePlus Real-Time PCR system (Life Technologies), using previously described primers (Decembre et al., 2014; Dreux et al., 2009). Extracellular and intracellular DENV, HCV and ZIKV RNA levels were normalized for Xef1α and GAPDH RNA levels, respectively.

Analysis of extracellular infectivity.

Infectivity titers in supernatants were determined by end-point dilution using Huh 7.5.1 cells. Foci forming unit (ffu) were detected 72 hours after infection by anti-HCV NS5A and anti- E glycoprotein specific immunofluorescence for HCV, DENV (clone 3H5), ZIKV (clone 4G2) respectively, as previously described (Decembre et al., 2014; Dreux et al., 2009). Briefly, Huh-7.5.1 cells were fixed with 4% PFA and permeabilized by incubation for 7 minutes in PBS containing 0.1% Triton. Cells were then blocked in PBS containing 3% BSA for 15 minutes and incubated for 1 hour with mouse anti-HCV NS5A (clone 9E10) diluted at 1:500 or mouse anti-DENV E glycoprotein (clone 3H5 or 4G2) hybridoma supernatant diluted at 1:200 in PBS containing 1% BSA. After 3 washes with PBS, cells were incubated 1 hour with secondary Alexa 555-conjugated anti-mouse antibody (2 µg/mL) and Hoechst dye in PBS containing 1% BSA. Percentage of NS5A-positive and E-positive cells cells was determined

using Zeiss Axiovert 135 or Olympus CKX53 microscopes.

QUANTIFICATION AND STATISTICAL ANALYSIS

Data are presented as the mean values ± standard deviation (SD). The figure legends report the number of independent experiments.

Statistical analysis was performed using R software environment for statistical computing and graphics, version 3.3.2. For levels of IFNα productions, viral RNA levels, viral titers and cell surface expression, the values were considered relative to untreated references for each independent experiment and analysis using an one-way ANOVA on ranks (Kruskal–Wallis test). When the test was significant, we used the Nemenyi *post hoc* test for multiple comparisons of mean rank sums to determine which contrast(s) between individual experimental condition pairs was significant. For the statistical analysis of polarization of structure/component at contact (assessed by confocal microscopy analysis), the distribution of the analyzed pDCs in contact with infected cells that presents co-clusters at the contact (without or with additional cluster outside contact) *versus* no co-cluster at contact (without or with cluster outside contact) were compared using Fisher's exact test for count data. Similar results were obtained when using the test for equality of proportions. Statistical analysis of viral transmission from GFP^- infected cells to GFP^+ uninfected cells was performed using one-way ANOVA, followed by Tukey multiple comparisons of means. The results of imaging flow cytometry (using Image Stream X technology) were analyzed using the Wilcoxon Unpaired test. For statistical analysis of the duration of contact (assessed by live-imaging using spinning-disk confocal microscopy analysis), a test for pairwise equality of proportions was applied to determine whether the duration of contact depends on the experimental conditions by comparing the frequency of the indicated time lengths. Data considered significant demonstrated adjusted p-value by False Discovery Rate (FDR) less than 0.05.

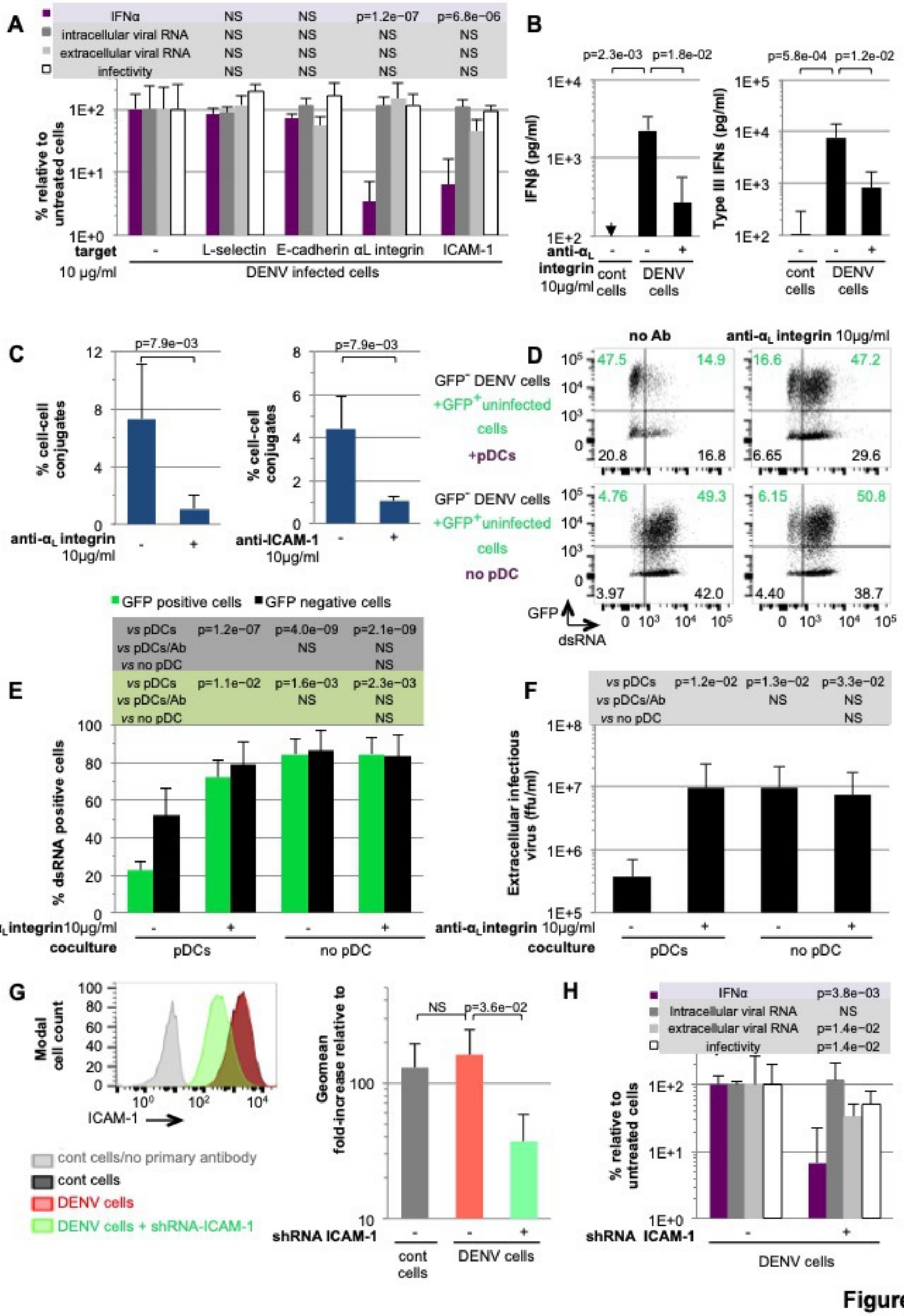
A
IFNα NS NS p=1.2e−07 p=6.8e−06
intracellular viral RNA NS NS NS NS
extracellular viral RNA NS NS NS NS
infectivity NS NS NS NS
% relative to untreated cells
1E+2
1E+1
1E+0
target - L-selectin E-cadherin αL integrin ICAM-1
10 µg/ml
DENV infected cells
B
p=2.3e-03 p=1.8e-02
IFNβ (pg/ml)
1E+4
1E+3
1E+2
anti-αL integrin 10µg/ml - - +
cont cells
DENV cells
p=5.8e-04 p=1.2e-02
Type III IFNs (pg/ml)
1E+5
1E+4
1E+3
1E+2
cont cells
DENV cells
C
p=7.9e−03
% cell-cell conjugates
12
8
4
0
anti-αL integrin 10µg/ml - +
p=7.9e−03
% cell-cell conjugates
8
6
4
2
0
anti-ICAM-1 10µg/ml - +
GFP positive cells GFP negative cells
vs pDCs p=1.2e−07 p=4.0e−09 p=2.1e−09
vs pDCs/Ab NS NS
vs no pDC NS
D
no Ab
anti-αL integrin 10µg/ml
GFP- DENV cells +GFP+ uninfected cells +pDCs
47.5 14.9 20.8 16.8
16.6 47.2 6.65 29.6
GFP- DENV cells +GFP+ uninfected cells no pDC
4.76 49.3 3.97 42.0
6.15 50.8 4.40 38.7
GFP
dsRNA
E
vs pDCs p=1.1e−02 p=1.6e−03 p=2.3e−03
vs pDCs/Ab NS NS
vs no pDC NS
% dsRNA positive cells
100
80
60
40
20
0
anti-αL integrin 10µg/ml - + - +
coculture pDCs no pDC
F
vs pDCs p=1.2e−02 p=1.3e−02 p=3.3e−02
vs pDCs/Ab NS NS
vs no pDC NS
Extracellular infectious virus (ffu/ml)
1E+8
1E+7
1E+6
1E+5
anti-αL integrin 10µg/ml - + - +
coculture pDCs no pDC
G
Modal cell count
100
80
60
40
20
0
ICAM-1
cont cells/no primary antibody
cont cells
DENV cells
DENV cells + shRNA-ICAM-1
Geomean fold-increase relative to
NS p=3.6e−02
100
10
shRNA ICAM-1 - - +
cont cells
DENV cells
H
IFNα p=3.8e−03
Intracellular viral RNA NS
extracellular viral RNA p=1.4e−02
infectivity p=1.4e−02
% relative to untreated cells
1E+2
1E+1
1E+0
shRNA ICAM-1 - +
DENV cells

Figure 1

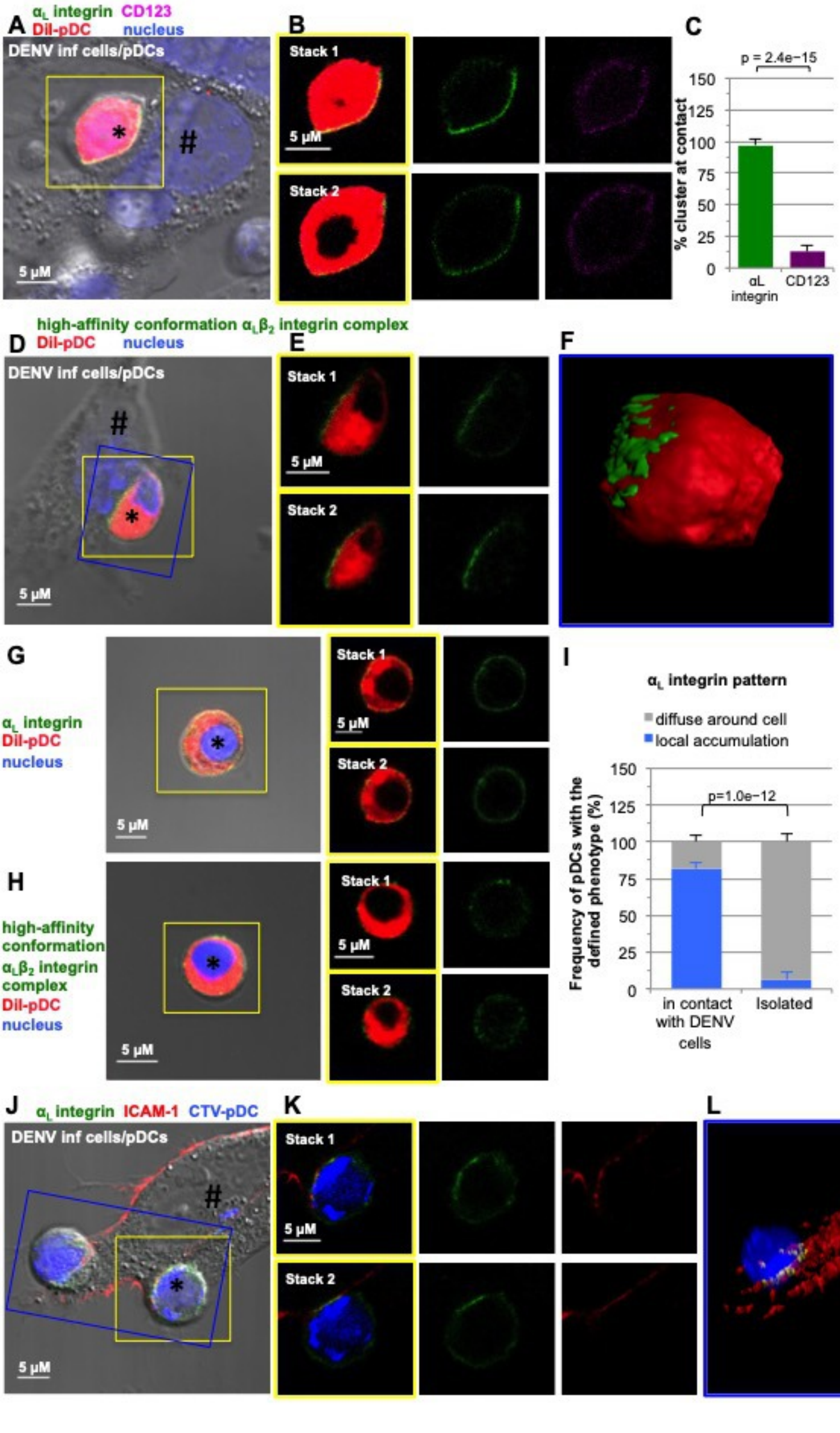
A
αL integrin CD123
DiI-pDC nucleus
DENV inf cells/pDCs
5 μM
B
Stack 1
Stack 2
5 μM
C
p = 2.4e−15
% cluster at contact
150
125
100
75
50
25
0
αL integrin
CD123
D
high-affinity conformation αLβ2 integrin complex
DiI-pDC nucleus
DENV inf cells/pDCs
5 μM
E
Stack 1
Stack 2
5 μM
F
G
αL integrin
DiI-pDC
nucleus
5 μM
Stack 1
Stack 2
5 μM
H
high-affinity conformation αLβ2 integrin complex
DiI-pDC
nucleus
5 μM
Stack 1
Stack 2
5 μM
I
αL integrin pattern
diffuse around cell
local accumulation
Frequency of pDCs with the defined phenotype (%)
150
125
100
75
50
25
0
p=1.0e−12
in contact with DENV cells
Isolated
J
αL integrin ICAM-1 CTV-pDC
DENV inf cells/pDCs
5 μM
K
Stack 1
Stack 2
5 μM
L

Figure 2

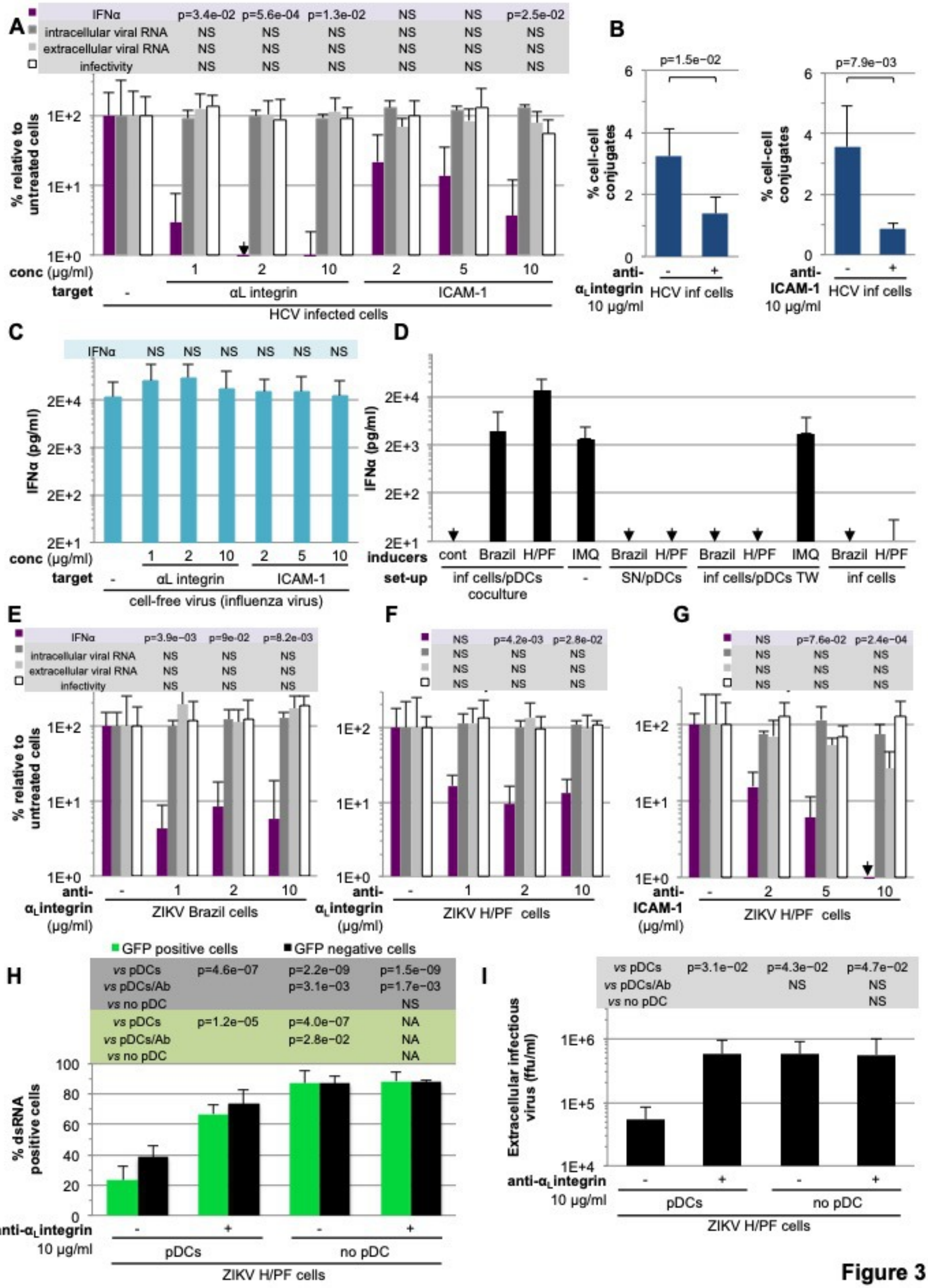
A
IFNα p=3.4e-02 p=5.6e-04 p=1.3e-02 NS NS p=2.5e-02
intracellular viral RNA NS NS NS NS NS NS
extracellular viral RNA NS NS NS NS NS NS
infectivity NS NS NS NS NS NS
% relative to untreated cells
1E+2
1E+1
1E+0
conc (µg/ml) 1 2 10 2 5 10
target - αL integrin ICAM-1
HCV infected cells
B
p=1.5e-02
% cell-cell conjugates
anti-αL integrin 10 µg/ml
HCV inf cells
p=7.9e-03
anti-ICAM-1 10 µg/ml
HCV inf cells
C
IFNα NS NS NS NS NS NS
IFNα (pg/ml)
2E+4
2E+3
2E+2
2E+1
conc (µg/ml) 1 2 10 2 5 10
target - αL integrin ICAM-1
cell-free virus (influenza virus)
D
IFNα (pg/ml)
inducers cont Brazil H/PF IMQ Brazil H/PF Brazil H/PF IMQ Brazil H/PF
set-up inf cells/pDCs coculture - SN/pDCs inf cells/pDCs TW inf cells
E
IFNα p=3.9e-03 p=9e-02 p=8.2e-03
intracellular viral RNA NS NS NS
extracellular viral RNA NS NS NS
infectivity NS NS NS
% relative to untreated cells
anti-αL integrin (µg/ml) - 1 2 10
ZIKV Brazil cells
F
NS p=4.2e-03 p=2.8e-02
NS NS NS
NS NS NS
anti-αL integrin (µg/ml) - 1 2 10
ZIKV H/PF cells
G
NS p=7.6e-02 p=2.4e-04
NS NS NS
NS NS NS
anti-ICAM-1 (µg/ml) - 2 5 10
ZIKV H/PF cells
GFP positive cells
GFP negative cells
H
vs pDCs p=4.6e-07 p=2.2e-09 p=1.5e-09
vs pDCs/Ab p=3.1e-03 p=1.7e-03
vs no pDC NS
vs pDCs p=1.2e-05 p=4.0e-07 NA
vs pDCs/Ab p=2.8e-02 NA
vs no pDC NA
% dsRNA positive cells
anti-αL integrin 10 µg/ml - + - +
pDCs no pDC
ZIKV H/PF cells
I
vs pDCs p=3.1e-02 p=4.3e-02 p=4.7e-02
vs pDCs/Ab NS NS
vs no pDC NS
Extracellular infectious virus (ffu/ml)
anti-αL integrin 10 µg/ml - + - +
pDCs no pDC
ZIKV H/PF cells

Figure 3

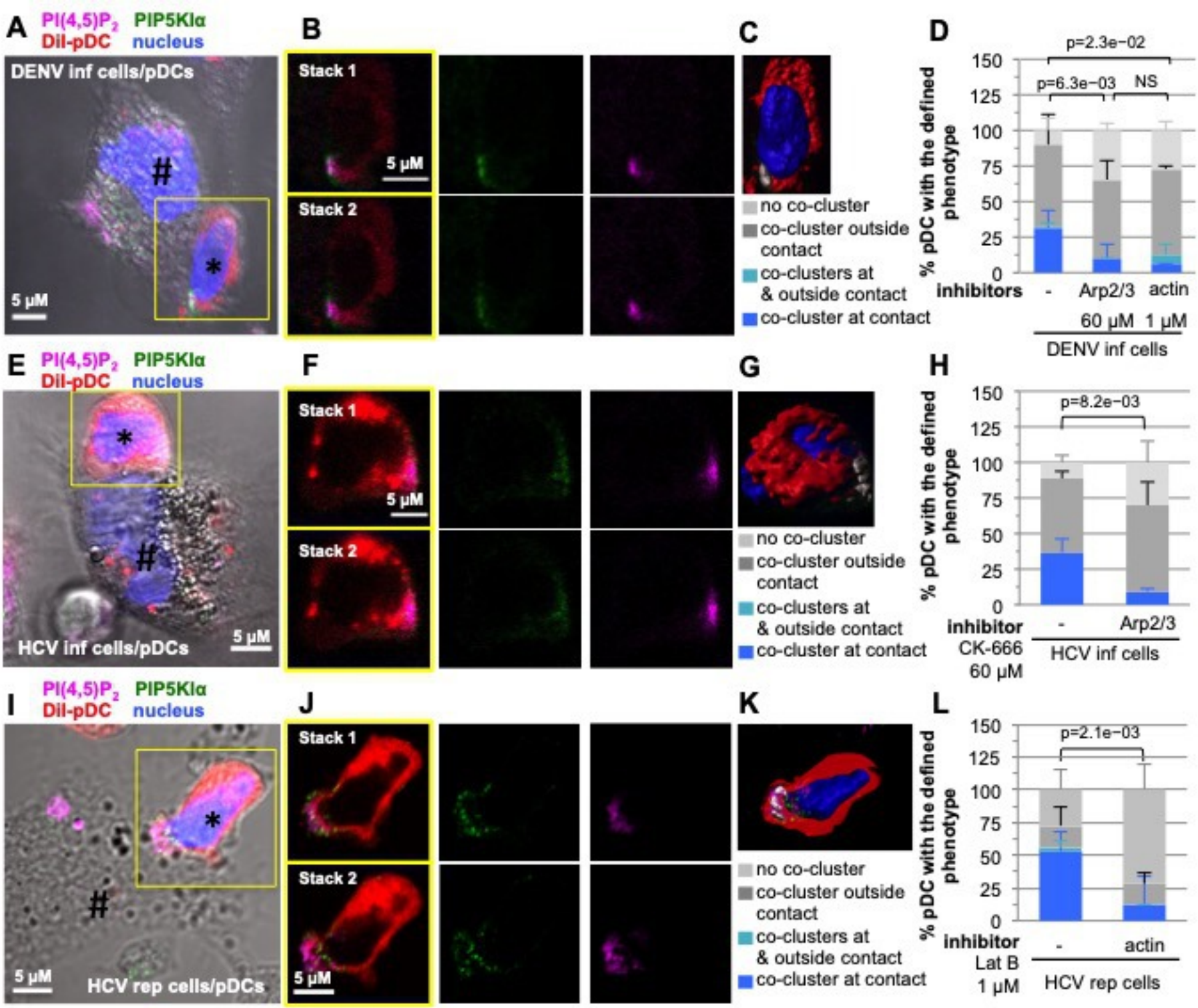
A
PI(4,5)P2
DiI-pDC
PIP5KIα
nucleus
DENV inf cells/pDCs
5 μM
B
Stack 1
Stack 2
5 μM
C
no co-cluster
co-cluster outside contact
co-clusters at & outside contact
co-cluster at contact
D
p=2.3e−02
p=6.3e−03
NS
% pDC with the defined phenotype
inhibitors
-
Arp2/3
actin
60 μM
1 μM
DENV inf cells
E
PI(4,5)P2
DiI-pDC
PIP5KIα
nucleus
HCV inf cells/pDCs
5 μM
F
Stack 1
Stack 2
5 μM
G
no co-cluster
co-cluster outside contact
co-clusters at & outside contact
co-cluster at contact
H
p=8.2e−03
% pDC with the defined phenotype
inhibitor
CK-666
60 μM
-
Arp2/3
HCV inf cells
I
PI(4,5)P2
DiI-pDC
PIP5KIα
nucleus
HCV rep cells/pDCs
5 μM
J
Stack 1
Stack 2
5 μM
K
no co-cluster
co-cluster outside contact
co-clusters at & outside contact
co-cluster at contact
L
p=2.1e−03
% pDC with the defined phenotype
inhibitor
Lat B
1 μM
-
actin
HCV rep cells
IFNα
intracellular viral RNA
extracellular viral RNA
M
IFNα NS p=1.9e-03
intracellular viral RNA NS NS
extracellular viral RNA NS NS
% relative to untreated coculture
Arp2/3 inh
CK-666, μM
DENV inf cells
N
IFNα p=2.2e-04 p=6.9e−07
intracellular viral RNA NS NS
extracellular viral RNA NS p=0.04
HCV inf cells
O
IFNα p=2e-02 p=6.8e-04
intracellular viral RNA NS NS
extracellular viral RNA NS NS
HCV rep cells
P
IFNα NS NS
IFNα (pg/ml)
Arp2/3 inh
CK-666, μM
cell-free influenza virus
Q
p=2.9e-02
p=2.9e-02
% cell-cell conjugates
DENV inf cells
R
p=1.6e-02
NS
% cell-cell conjugates
HCV inf cells

Figure 4

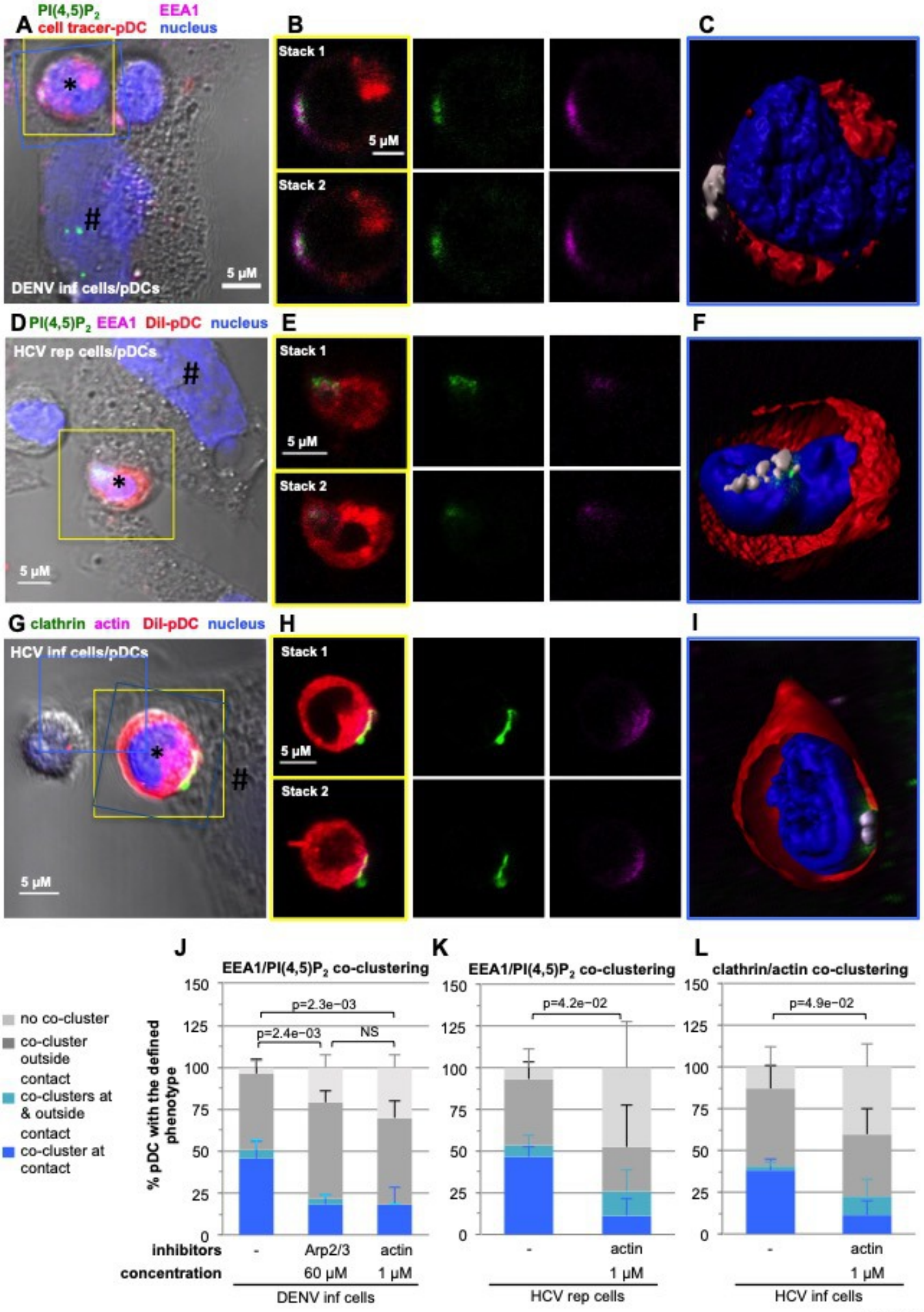
A
PI(4,5)P2
cell tracer-pDC
EEA1
nucleus
DENV inf cells/pDCs
5 μM
B
Stack 1
Stack 2
5 μM
C
D
PI(4,5)P2 EEA1 DiI-pDC nucleus
HCV rep cells/pDCs
5 μM
E
Stack 1
Stack 2
5 μM
F
G
clathrin actin DiI-pDC nucleus
HCV inf cells/pDCs
5 μM
H
Stack 1
Stack 2
5 μM
I
J
EEA1/PI(4,5)P2 co-clustering
p=2.3e−03
p=2.4e−03
NS
K
EEA1/PI(4,5)P2 co-clustering
p=4.2e−02
L
clathrin/actin co-clustering
p=4.9e−02
no co-cluster
co-cluster outside contact
co-clusters at & outside contact
co-cluster at contact
% pDC with the defined phenotype
150
125
100
75
50
25
0
inhibitors
concentration
-
Arp2/3
60 μM
actin
1 μM
DENV inf cells
HCV rep cells
HCV inf cells

Figure 5

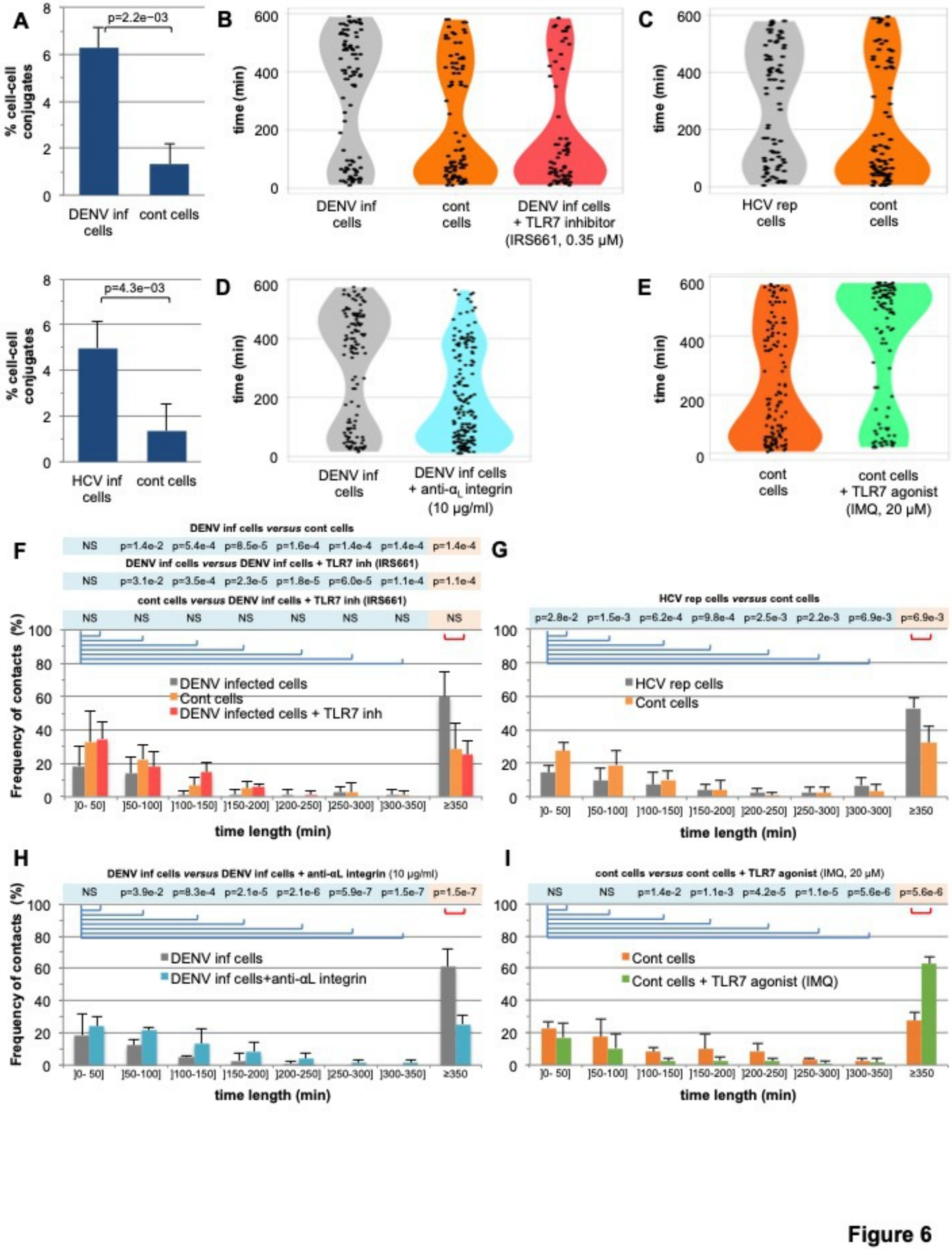
A
p=2.2e−03
% cell-cell conjugates
DENV inf cells
cont cells
B
time (min)
DENV inf cells
cont cells
DENV inf cells + TLR7 inhibitor (IRS661, 0.35 µM)
C
time (min)
HCV rep cells
cont cells
p=4.3e−03
% cell-cell conjugates
HCV inf cells
cont cells
D
time (min)
DENV inf cells
DENV inf cells + anti-αL integrin (10 µg/ml)
E
time (min)
cont cells
cont cells + TLR7 agonist (IMQ, 20 µM)
F
DENV inf cells versus cont cells
NS p=1.4e-2 p=5.4e-4 p=8.5e-5 p=1.6e-4 p=1.4e-4 p=1.4e-4 p=1.4e-4
DENV inf cells versus DENV inf cells + TLR7 inh (IRS661)
NS p=3.1e-2 p=3.5e-4 p=2.3e-5 p=1.8e-5 p=6.0e-5 p=1.1e-4 p=1.1e-4
cont cells versus DENV inf cells + TLR7 inh (IRS661)
NS NS NS NS NS NS NS NS
Frequency of contacts (%)
DENV infected cells
Cont cells
DENV infected cells + TLR7 inh
]0- 50]
]50-100]
]100-150]
]150-200]
]200-250]
]250-300]
]300-350]
≥350
time length (min)
G
HCV rep cells versus cont cells
p=2.8e-2 p=1.5e-3 p=6.2e-4 p=9.8e-4 p=2.5e-3 p=2.2e-3 p=6.9e-3 p=6.9e-3
HCV rep cells
Cont cells
]0- 50]
]50-100]
]100-150]
]150-200]
]200-250]
]250-300]
]300-300]
≥350
time length (min)
H
DENV inf cells versus DENV inf cells + anti-αL integrin (10 µg/ml)
NS p=3.9e-2 p=8.3e-4 p=2.1e-5 p=2.1e-6 p=5.9e-7 p=1.5e-7 p=1.5e-7
Frequency of contacts (%)
DENV inf cells
DENV inf cells+anti-αL integrin
]0- 50]
]50-100]
]100-150]
]150-200]
]200-250]
]250-300]
]300-350]
≥350
time length (min)
I
cont cells versus cont cells + TLR7 agonist (IMQ, 20 µM)
NS NS p=1.4e-2 p=1.1e-3 p=4.2e-5 p=1.1e-5 p=5.6e-6 p=5.6e-6
Cont cells
Cont cells + TLR7 agonist (IMQ)
]0- 50]
]50-100]
]100-150]
]150-200]
]200-250]
]250-300]
]300-350]
≥350
time length (min)

Figure 6

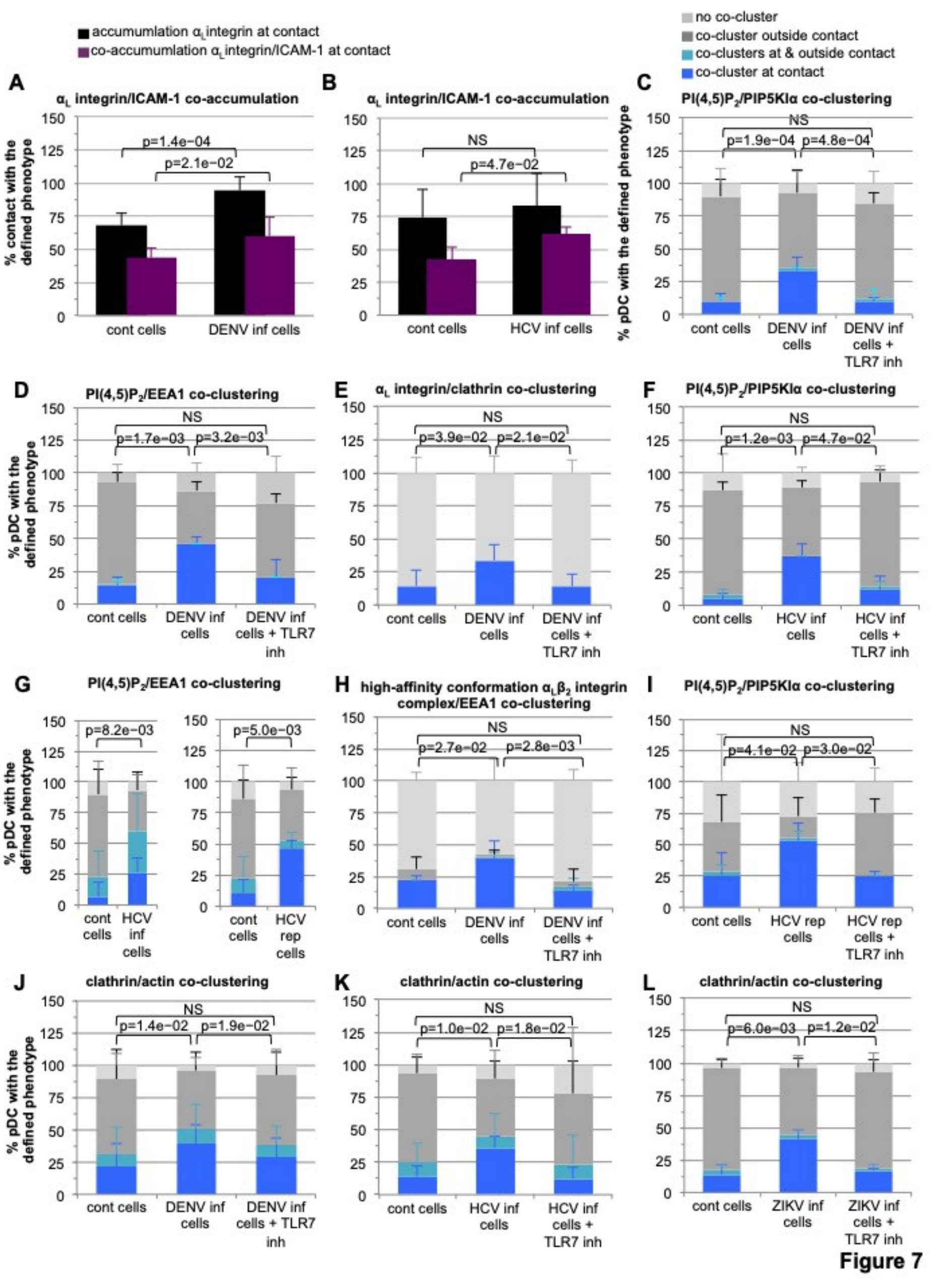
accumumlation αL integrin at contact
co-accumumlation αL integrin/ICAM-1 at contact
no co-cluster
co-cluster outside contact
co-clusters at & outside contact
co-cluster at contact
A
αL integrin/ICAM-1 co-accumulation
% contact with the defined phenotype
p=1.4e−04
p=2.1e−02
cont cells
DENV inf cells
B
αL integrin/ICAM-1 co-accumulation
NS
p=4.7e−02
cont cells
HCV inf cells
C
PI(4,5)P2/PIP5KIα co-clustering
% pDC with the defined phenotype
NS
p=1.9e−04
p=4.8e−04
cont cells
DENV inf cells
DENV inf cells + TLR7 inh
D
PI(4,5)P2/EEA1 co-clustering
% pDC with the defined phenotype
NS
p=1.7e−03
p=3.2e−03
cont cells
DENV inf cells
DENV inf cells + TLR7 inh
E
αL integrin/clathrin co-clustering
NS
p=3.9e−02
p=2.1e−02
cont cells
DENV inf cells
DENV inf cells + TLR7 inh
F
PI(4,5)P2/PIP5KIα co-clustering
NS
p=1.2e−03
p=4.7e−02
cont cells
HCV inf cells
HCV inf cells + TLR7 inh
G
PI(4,5)P2/EEA1 co-clustering
% pDC with the defined phenotype
p=8.2e−03
p=5.0e−03
cont cells
HCV inf cells
cont cells
HCV rep cells
H
high-affinity conformation αLβ2 integrin complex/EEA1 co-clustering
NS
p=2.7e−02
p=2.8e−03
cont cells
DENV inf cells
DENV inf cells + TLR7 inh
I
PI(4,5)P2/PIP5KIα co-clustering
NS
p=4.1e−02
p=3.0e−02
cont cells
HCV rep cells
HCV rep cells + TLR7 inh
J
clathrin/actin co-clustering
% pDC with the defined phenotype
NS
p=1.4e−02
p=1.9e−02
cont cells
DENV inf cells
DENV inf cells + TLR7 inh
K
clathrin/actin co-clustering
NS
p=1.0e−02
p=1.8e−02
cont cells
HCV inf cells
HCV inf cells + TLR7 inh
L
clathrin/actin co-clustering
NS
p=6.0e−03
p=1.2e−02
cont cells
ZIKV inf cells
ZIKV inf cells + TLR7 inh

Figure 7

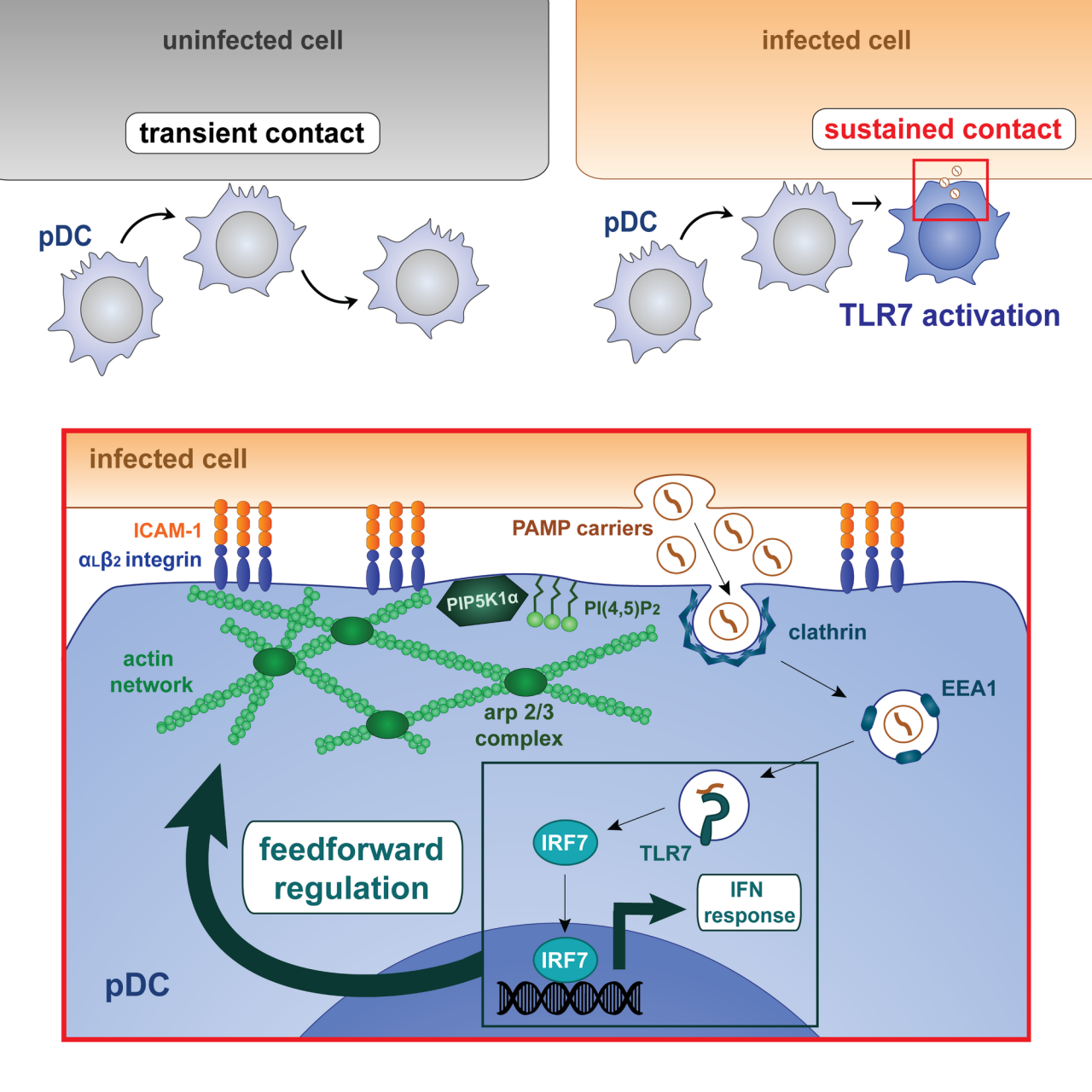
uninfected cell
transient contact
pDC
infected cell
sustained contact
pDC
TLR7 activation
infected cell
ICAM-1
αLβ2 integrin
PAMP carriers
PIP5K1α
PI(4,5)P2
clathrin
actin
network
arp 2/3
complex
EEA1
feedforward
regulation
IRF7
TLR7
IFN
response
IRF7
pDC